ALMA MATER STUDIORUM - UNIVERSITÀ DI BOLOGNA

FACOLTA' DI INGEGNERIA

CORSO DI LAUREA IN INGEGNERIA CIVILE

D.I.C.A.M.

TESI DI LAUREA

Geotecnica Applicata

Behaviour of Monopod Bucket Foundations Under Horizontal Load in Dense Sand

CANDIDATO

Aligi Foglia

RELATORE

Guido Gottardi

CORRELATORI

Lars Bo Ibsen
Alberto Lamberti

Anno Accademico 2010/2011

Sessione I

Chapter 1

Introduction

Over the last 20-years period, research has focused more and more on renewable energy systems, to decrease the global warming hazard. Among such technologies, wind energy takes place strongly with two options: onshore and offshore wind turbines. Both of them have been quickly developed during last two decades because, in spite the high installation, operation and maintenance costs they do not have a big impact on the environment and are easily decommissioning.

At the very beginning of the wind energy life, in the early 90's, European countries such as Denmark, Germany and United Kingdom, focused on windiest land-areas for the installation of 300-500 kW wind turbines, for domestic energy supply purposes. The height of the first wind energy converter installed was around 40 m, and the power production was 550 kW (U.S. En. Dep., 2007). Over the past two decades wind energy has been subjected to a quite significant development and currently the largest wind energy converter in the world takes place in Belgium and has an outstanding height of 135m with a turbine working at 7 MW of energy output.

One of the problems of land based wind plants is that often sites with strong wind available are very distant from the main urban centres. Indeed it is commonly known that wind increases when no obstacles are on its way. In addition the exploitation of land based wind resource can be forbidden, because of planning procedures and other institutional obstacles. This means that, the ideal places for wind farms are likely to be located in the more remote areas where grid connection may be difficult. Other problems of land based wind farms are the noise of the rotor, the aesthetic impact, and furthermore, the difficulty of large pieces transport.

On the other hand, at the sea wind blows steadier and faster. Generally the farer a site is from the coast the stronger the wind blows. Although, being this wind rise quick, wind farms can be installed within a reasonable distance from the coast. In addition no limitation is given to the size of transported pieces. For these reasons sea seems to be the ideal place for wind turbine converters. Thus, offshore wind energy has the potential to be a great renewable energy resource for the future even thinking that, all over

the world, coastlines are locations whereon large urban centres take place (Musial *et al.*, 2006).

In 1991 Denmark was the first country ever dealing with offshore wind energy. After this first attempt other European countries have undertaken many other projects. The current world-wide status of energy production, by means of offshore wind systems, is shown in Figure 1.1. As one can notice most of the countries involved are European, however the current status will not last for long since a massive grown of the wind turbine market is expected in next years.

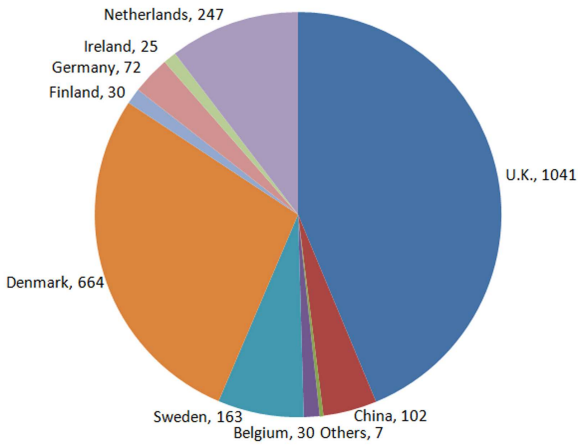

Figure 1.1: MW of energy generated by offshore wind farms (U.S. En. Dep., 2007).

Germany, United Kingdom and Denmark will be among the European countries taking a lead in the development of the offshore wind power. By 2050 50 % of the total European energy consumption is likely to be provided by wind. The market is raising more and more with about 1000 MW to be installed within 2010 and 50.000 MW for 2011 and further years only among European countries. It is outstanding thinking how such a rise of offshore wind turbines installation is going to happen in few years with a growing rate never seen before (NREL, 2010).

Looking at extra-European countries, Canada China and United States seem to be the most interested nations in planning offshore wind farms on their sea areas. United States (that have always led the onshore wind resources) have the ambitious goal of reaching 54 GW of electricity power, provided by offshore wind turbines by 2030. United States will be mostly focused on Gulf of Mexico, Great Lakes and the Pacific Cost as installation areas. India has an

ambitious aim too which is, reaching 3 % of the total electricity consumption by using land-based wind turbines within the next decade (Banks, 2010).

The major current challenge of offshore wind engineering is to lower costs. Logistic and support structure costs can be up to the 25 % of the overall cost. Therefore both installation and foundation technologies must be investigated in order to find new cost-effective ways. Below is showed a typical cost breakdown for a baseline offshore wind turbine.

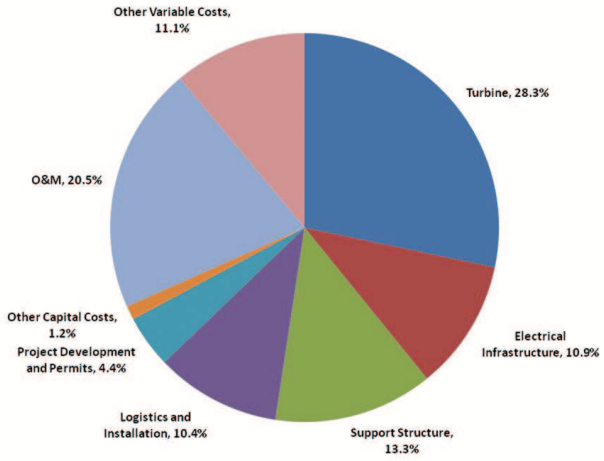

Figure 1.2: Cost breakdown for a baseline offshore wind turbine (NREL, 2010).

1.1 Support Structure Concepts

This section will not provide a complete chart of offshore foundation types. In the following only a brief explanation of the most common technologies will be considered. Besides, it is worth saying that, every construction company may have its own particular technology for both installation procedure and foundation design systems. Thus, the following section has to be taken as general and not specific indication.

Offshore support structures can be categorized in monopod and multipod supports as it is depicted in Figure 1.3.

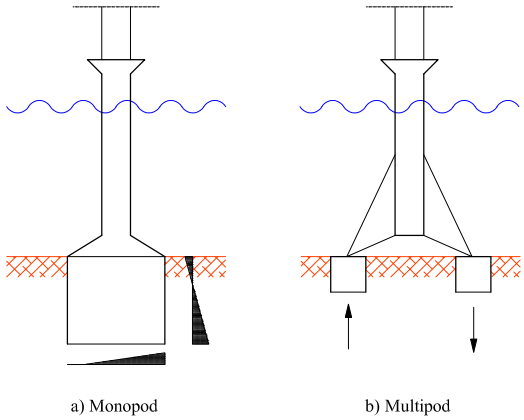

Figure 1.3: Monopod and multipod technology with relative foundations reactions, after (LeBlanc, 2009).

The main difference between the two concepts is how the moment is transferred to the soil. While monopods transfer the loading moment only by one interface with the surrounding soil, multipods transfer the moment applied by a simultaneous compression-tension action. Both monopods and multipods can have either gravity, monopile or suction caisson as foundation structures. Multipod foundations are cost-effective in water depth larger than 25-30 m. At such depths a monopod foundation would require a large amount of material to reach the needed stiffness.

By far, gravity and pile foundations have been the most used support structures for offshore wind turbines. The main reason of their usage relies on the fact that both pile and gravity foundations are considered reliable since they have been experienced for decades with a lot of different purposes. The most significant shortcoming, related to these support technologies, is the high cost of construction and installation. Gravity foundations require large amount of concrete, heavy vessels for installation, near sources of ballast material and a long time for seabed preparation. Monopiles need high quantity of steel as well as heavy installation vessels and very expensive hydraulic hammer for penetrating the seabed. Hence, it is clear that cost-effective solutions must be addressed. A valid and cost-effective alternative for next generations of offshore wind turbines support may be the suction caisson foundation.

1.2 Suction Caisson Foundation

This thesis will focus on the investigation of suction caisson as foundation for offshore wind turbines. In the following the concept and installation of such foundation are described.

1.2.1 General Features and Installation

Suction caisson or suction bucket foundations are basically composed of three parts (illustrate in Figure 1.4): skirt, lid and upper piece.

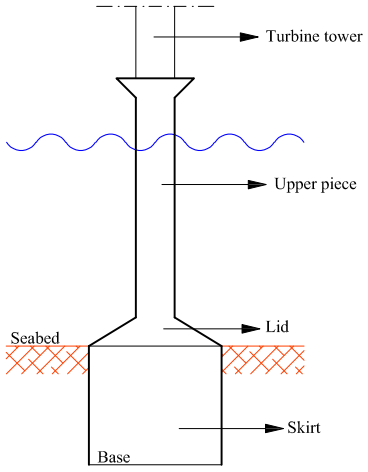

Figure 1.4: Components of suction caisson foundation.

The skirt is the only interface with the soil, therefore a fully understanding of its behaviour is essential for a correct foundation design. The lid is the connection part between skirt and upper pile. This connection is provided by means of a large reinforced steel structure. Such structure is meant for transferring loads from the column to the skirt edges. The upper pile is placed on the lid and the turbine tower is mounted on it.

Most of the times the installation procedure of a caisson foundation is less technically challenging than that of the monopile or gravity foundation. In fact, heavy vessels are avoidable since floating self-installing bucket have been proved, cf. Figure 1.5. Besides, the entire installation is likely to be carried out in a few hours and be less weather-dependent (Houlsby and

Byrne, 2002). Moreover suction caissons may be a good alternative for large diameter monopiles that sometimes are hardly drivable into the seabed. Also the structure itself may cost less. Indeed, in spite a costly lid, the total amount of steel needed can be less than that of the monopile. For such reasons, when appropriate soil conditions and reliable penetration methods are offered, the suction caisson technology becomes convenient in terms of cost and time. The scour protection is a relevant issue related to this kind of foundation, thus high priority is placed on investigating mitigation methods.

Figure 1.5: Floating bucket foundation (LeBlanc, 2009).

The method used for penetrating the bucket into seabed is nearly the same for any soil. What differs during penetration is the behaviour of different soils (clay, sand, silt) due to suction. In other words the skirt penetrates in different soils through different effects.

The penetration of the bucket into the seabed can be simplified in two steps as shown in Figure 1.6. Initially penetration begins by means of the self weight of the structure. Subsequent penetration is provided by a pump which creates suction pressure. The pressure leads to the suction penetration of the skirt bottom. The skirt penetrates into the soil because the effective stress below the skirt tip decreases, due to the waterflow, which allows for a reduction of the penetration resistance.

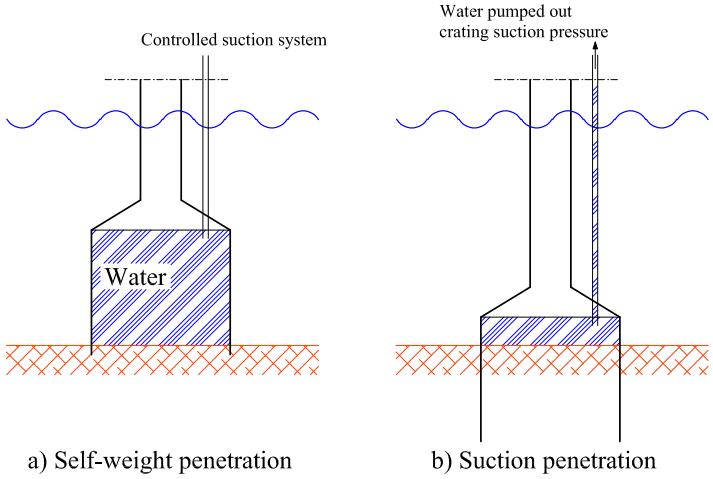

Figure 1.6: Installation phases for suction caisson.

The installation requires considerable care, because stones or rocks can be met by the skirt on its way down. This can induce an inclination which is dealt with by applying pressure inside the bucket. Thereby the bucket is brought to horizontal position and further installation can be carried out. If the stone or rock is considerably large the entire installation is compromised.

Another vital aspect of the installation is the possible creation of piping channels, which occurs when the critical gradient (which depends on the effective unit weight of soil) is overcome. This means that the suction pressure should be kept at the minimum. If piping channels occur the suction must stop and further soil should be added to the piping area. When pore pressure has dissipated, the penetration session can restart. The horizontal alignment during installation is subjected to a strict requirement because the deflection of the turbine tower can seriously compromise the turbine efficiency. Thus, the horizontal level of the caisson during installation must be monitored. When the target depth is reached the pump stops, and the pumping system is dismantled. The decommissioning procedure is similar to the installation, the overall process is simply reverse.

As any other monopod support structure, suction caissons are mainly subjected to a moment loading at the seabed and relatively low vertical forces. The bearing moment capacity of this foundation is basically dependent on the skirt length and on the caisson diameter. One of the basic ideas is that

bucket foundations can be considered similar to embedded circular foundations because of the inner soil trapped which acts as a rigid cluster. Of course, in such case the roughness of the base must be considered.

1.2.2 Recent Studies on Bucket Foundations

Lately, understanding the behaviour of suction caissons has received many improvements, by both theoretical and practical research. Larsen (2008) achieved interesting results about vertical bearing capacity and yield surface of combined loading. He performed more than 100 tests in large and small-scale creating a consistent database to develop and/or confirm theories. Thereafter he compared test results with a FE-method and with methods found in literature. In contrary to most of the previous studies conducted on bucket foundations tests were performed with constant vertical load. Moreover every tests was carried out until failure of the soil occurred. Terzaghi's bearing capacity formula was found able to assess the vertical bearing capacity of bucket foundations. A new equations describing the bearing capacity factors was put forward by using FE-codes (calibrated through small-scale tests). The yield criterion proposed by Villalobos *et al.* (2004) was modified to account for the different vertical loads applied. A linear failure criterion regarding low vertical load was set out. Embedment ratio and load path were assessed to be affecting the failure parameters. The serviceability behaviour (not up to failure) was found to be affected by embedment ratio and load path as well. Observations regarding the hardening law were also presented.

Over the last decade Oxford University has been developing a programme of research aimed at offshore wind turbine design. High priority has been placed on lowering the installation price and defining design frameworks (Houlsby and Byrne, 2002). Small and large-scale tests were conducted and both monopod and tripod (or quadruped) solutions were addressed. Most relevant for the multipod foundations is the behaviour under monotonic or cyclic vertical loading. Such behaviour was investigated in papers such as Kelly *et al.* (2006b). However, more important for this thesis is the monopod foundation concept. The most significant papers regarding that are briefly outlined in the following.

The loading rig used (illustrated in Figure 1.10) for small-scale experiments was designed at Oxford University initially to test foundation on clay. Further modifications to suit the purpose were actuated by Byrne (2000). The apparatus finally adopted was able to apply an arbitrary displacement path by using computer-controlled stepped motors. Vertical, horizontal and mo-

ment loading could independently be enforced to the system whilst the displacement of the foundation were measured by means of a displacement transducers system.

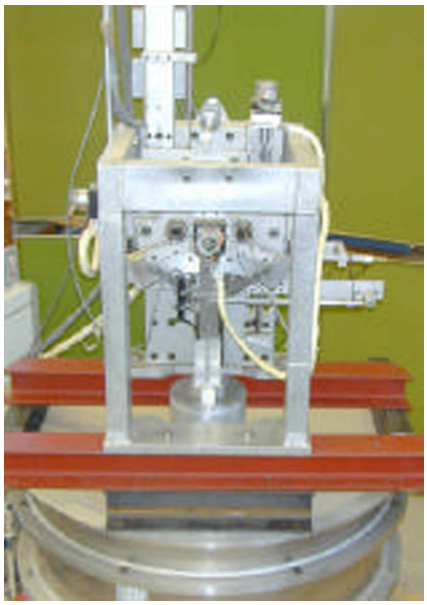

Figure 1.7: Experimental rig (Byrne *et al.*, 2003).

In Houlsby (1999) every experiment was interpreted within the plasticity theory framework. Records from monotonic loading tests were to some extend well fitted within the existing framework developed by Gottardi *et al.* (1999) . Conversely, records from cyclic loading tests shown that conventional plasticity models could not utterly represent data. A continuous hyperplastic model was finally adopted to capture the behaviour of cyclic tests. A remarkable result obtained can be seen in Figure 1.8 where rotational displacement against moment load by applying the plasticity theory, Figure 1.8 a), and by plotting one record from tests, Figure 1.8 b), are shown. In the latter article were pointed out also similarities between monotonic and cyclic loading at small displacement. Further information about the continuous hyperplastic model are available in Byrne *et al.* (2003) where monotonic vertical loading and moment loading tests are presented and interpreted in order to give preliminary indications to estimate the ultimate moment capacity and the installation procedure.

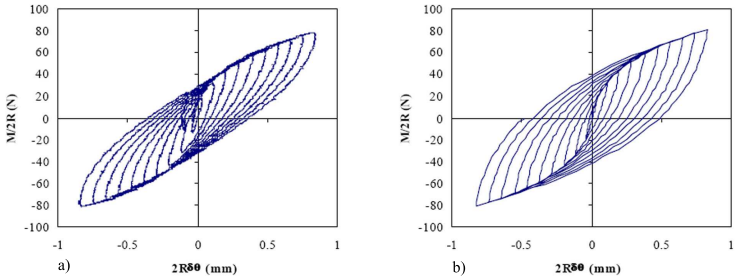

Figure 1.8: Comparison of laboratory tests a) and plasticity theory b) (Byrne *et al.*, 2003).

Field trials were also conducted in a bid to confirm laboratory test interpretation (Houlsby, 2006). The test equipment used is depicted in Figure 1.9. Two types of caissons were tested: diameter 3 m, skirt length 1.5 m, diameter 1.5 m, skirt length 1 m. Forces were applied by means of hydraulic jacks. Installation features, cyclic vertical loading and cyclic horizontal loading were mainly addressed. A relevant result achieved was the gradual reduction of stiffness with load amplitude cyclic moment as well as for cyclic vertical forces.

Laboratory tests were compared to field tests in Kelly *et al.* (2006a). In order to compare results from differently scaled tests particular dimensionless equations were employed. All in all, results at different scale, were fairly comparable by applying scaling relationship. Although, some quantitative results regarding the displacement accumulation could not be perfectly replicated. Cyclic loading was studied by means of a novel loading rig. This will be presented in Chapter 2.

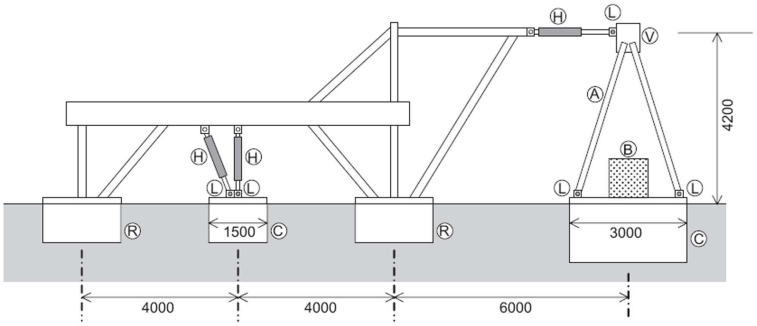

Figure 1.9: Field trials equipment (Houlsby, 2006).

The University of Western Australia investigated suction caisson foundations focusing on several topics. Doherty and Deeks (2003) obtained stiffness coef-

ficients for rigid circular footings by using the scaled boundary FEM (representing an elastic half-space). The effect of the non-homogeneous parameter α on the stiffness parameters were mainly addressed. In Doherty *et al.* (2004) the scaled boundary FEM was used again combined with shell finite element representing the caisson. The stiffness was found dependent on the skirt flexibility. Recently, Senders (2008) has carried out research on suction caisson as tripod foundation. A computer programme to predict loading conditions of a tripod foundation was improved. Small scale tests were performed by utilizing centrifuge device. Vertical cyclic loading was investigated.

Still, many unsolved problems are related to suction caisson foundations, such as the influence of both the vertical tension and the relative density, and nonetheless the presence of layered soils. However, these are not of major interest for this thesis, which will instead focus on the horizontal load-displacement behaviour, as a preliminary research for further cyclic loading studies.

1.3 Aim of the thesis

This thesis aims at finding, through small-scale tests, consistent relationships load-displacement to be employed in predicting the real-scale behaviour of a bucket foundation. This is attempted by looking through data from small-scale tests of bucket foundations, and interpreting them on the base of a similitude theory. The case of study is a monopod bucket foundation subjected to horizontal monotonic loading.

The main purpose of the study is to give a reliable preliminary base for further long term cyclic loading researches. Therefore, attention is mostly given to forces not up to the soil failure, as required by the fatigue limit states design (DNV, 2004). The overturning moment-rotation relationship and, thereof, the accumulated rotation of the bucket are top priorities in the fatigue limit states design.

The main content of the thesis is set out in two chapters. Chapter 4 presents a similitude theory, between small and large-scale, of the bucket foundation behaviour. The relationship sought is the horizontal load-displacement of the bucket. The theory is analytically demonstrated and then corroborated by analysing static small-scale tests of bucket foundations and triaxial tests data. The laboratory tests of bucket foundations were conducted by Larsen (2008) while the triaxial tests by Ibsen*et al.* (1995). Also the overturning

moment-rotation relationship is object of investigation.

In a bid to understand the effect of the overburden pressure on the relationships, Chapter 7 displays six further tests conducted on one bucket at different soil effective stress. To increase the effective stress a novel method was adopted.

A summary of the study is given in Figure 1.10.

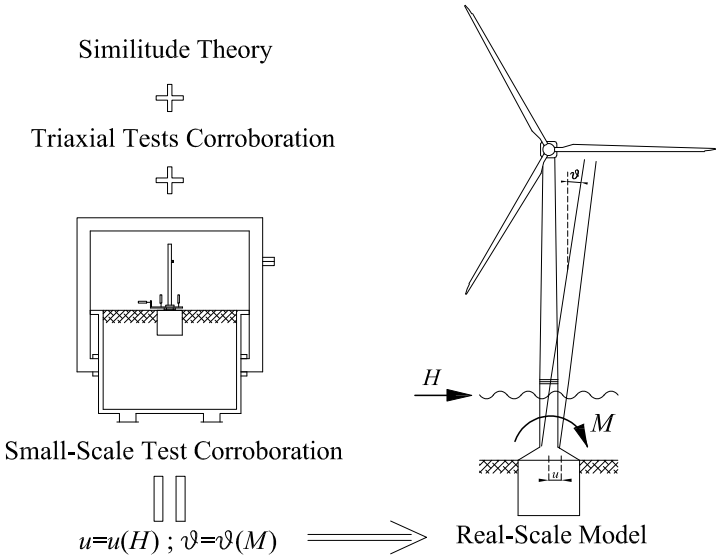

Figure 1.10: Summary of the study.

Chapter 2

Cyclic Loading on Offshore Structures

The main loads acting on an offshore wind energy structure are of two kinds: operational and environmental. Operational loads can be calculated with sufficient accuracy, while environmental loads are based on statistical measurements. The latter are affected by a certain uncertainty. Among environmental forces wind and wave account for 80-90 % of the total horizontal load acting on offshore wind turbines. The remaining percentage is attributed to sea currents and blade movements. Waves and winds are naturally cyclic, consequently, a wind turbine is exposed to millions of cycles over its lifetime. For this reason investigating the wind turbine foundations behaviour, under cyclic loading, shall be evaluated as essential. Certainly, numerous problems are related with cyclic loading such as changing of stiffness and accumulated deformations. In the worst case the natural frequency of the structure can get close to the resonance, or a distorted horizontal alignment can seriously affect the turbine efficiency. By leading research on cyclic loading, these circumstances will be avoided and a straightforward framework for fatigue design may be achieved .

Whilst there are already available guidance regarding the response of offshore foundations under monotonic loads, less emphasis has been given to the cyclic loading behaviour. Piles, for instance, are usually designed considering the p-y curves, adopted by DNV (2004) (which are the current avant-garde of offshore wind turbine standards) with the primary purpose of calculating the ultimate lateral capacity of a pile. Also for cyclic loading, DNV standards provided a p-y curve. However, these design rule is not capable to properly account for cyclic loading because nor number of cycles, neither load characteristics, are taken into consideration. These latter two cyclic load features should be considered as key issues of the fatigue design. A special regard should be given to them in further design methods. In the next section a state of the art about cyclic loading is presented.

2.1 Researches on Cyclic Loading, a State-of-the-Art

As yet, researches on offshore wind turbine foundations under cyclic loading have concerned mostly monopiles. Only few papers have investigated suction caissons. In the following the most relevant conclusions gained in the last five-year period are presented. All cited articles give a basic and general overview on the topic and have been source of inspiration for this thesis.

Degradation of Stiffness Method (DSM)

Drained cyclic triaxial tests on cohesionless soil and finite element analysis are the essential components of the DSM. This approach was put forward by Achmus *et al.* (2008). The purpose of the study was to give a preliminary design chart for cyclically loaded monopiles, installed in sand.

A previous research on monotonic loading was used for defining the secant modulus of elasticity E_s and assessing the stress conditions of every element. The assumed equation for E_s was:

$$E_s = k \cdot \sigma_{at} \cdot \left(\frac{\sigma_m}{\sigma_{at}}\right)^{\lambda} \tag{2.1}$$

wherein σ_{at} is the atmospheric pressure, σ_m the mean principal stress of elements, and k and λ are material constants.

An intuitive representation of the stiffness degradation of soil after a certain number of cycles N was given, cf. Figure 2.1.

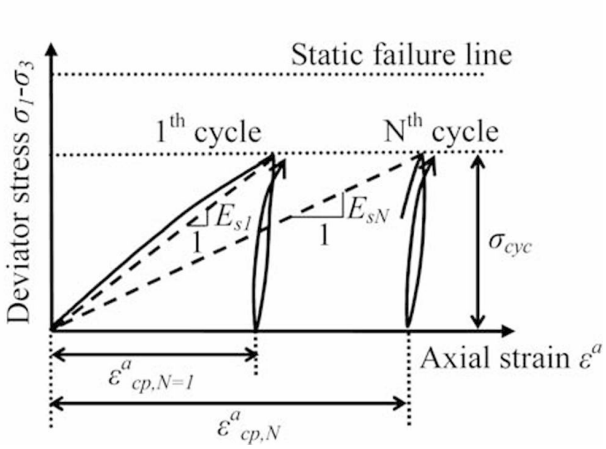

Figure 2.1: Degradation of stiffness after N cycles. (Achmus *et al.*, 2008).

According to Figure 2.1, equation (2.2) which relates secant stiffness modulus ratio to stress ratio was provided.

$$\frac{E_{sN}}{E_{s1}} \cong \frac{\varepsilon_{cp,1}}{\varepsilon_{cp,N}} \tag{2.2}$$

In equation (2.2) E_{sN}/E_{s1} is the ratio between secant elastic modulus at N^{th} and first cycle while $\varepsilon_{cp,1}/\varepsilon_{cp,N}$ is the ratio between plastic axial strain at first and N^{th} cycle.

Since equation (2.2) involves the accumulation of strain, an estimation of that was provided as well. Many semi-empirical approaches exist in literature, in this case Huurman's formula was used (Huurman, 1996).

$$\frac{E_{sN}}{E_{s1}} \cong \frac{\varepsilon_{cp,1}}{\varepsilon_{cp,N}} = N^{-b_1(X)^{b_2}} \tag{2.3}$$

where b_1 and b_2 are material parameters, and $X = \sigma_{1,cyc}/\sigma_{1,sf}$ was defined as cyclic stress ratio between the mayor principle stress for the cyclic stress state and the mayor principal stress at static failure state. Seeing that, in contrary to the real situation in-situ, the confining pressure is constant in triaxial tests, the cyclic stress ratio X was modified as follows:

$$X_c = \frac{X^1 - X^0}{1 - X^0} \tag{2.4}$$

The new defined ratio was named characteristic cyclic stress ratio and accounted for the anisotropic initial stress of the soil. The components X^1 and

X^0 indicate the cyclic stress ratio at loading and unloading phase respectively. Introducing the above conditions in the finite element analysis the degradation of stiffness method was complete. A significant result obtained by employing DSM was the deflection-No of cycles curve, cf. Figure 2.2.

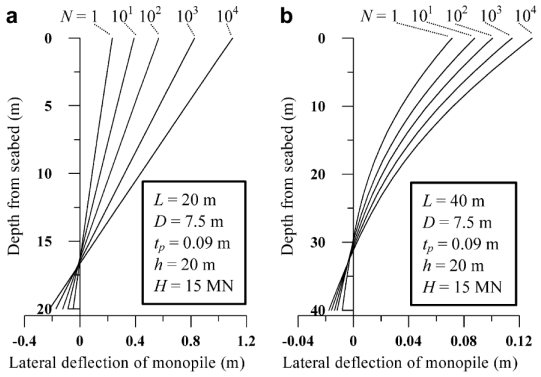

Figure 2.2: Deflection-No of cycles curve. (Achmus *et al.*, 2008).

The DSM was adopted for some parametric studies, which pointed out that the displacement accumulation due to cyclic loading was, to a large extent dependent on the embedment ratio, and slightly dependent on the pile diameter. By employing DSM specific cases could be studied, the magnitude of the load, and any other boundary condition of the problem could be controlled.

As mentioned before the design standards are based on *p-y* curves or on complicated material laws. Drawback of these approaches, is the quite limited application since they are not dependent nor on the number of cycles neither on the load features. The DSM is of course a step forward in comparison to the rough methods adopted in the standards. However, it is worth noticing that, nor small scale, neither large scale tests, have been used for calibrating the method. Indeed, only triaxial tests were conducted. Thus, the reliability of DSM needs many more studies to be proved.

LeBlanc's Approach

LeBlanc *et al.* (2010a) led research on rigid driven piles subjected to cyclic loading in a radically different way than the DSM. A series of long term cyclic loading on small-scale driven piles were conducted. Test results were afterwards scaled by means of a non-dimensional framework.

A long-term cyclic loading rig was used for conducting the experiments. The

top of the driven pile was loaded by a cyclic horizontal force which in turn created a moment acting on the ground surface. For uniquely describing the loading moment two parameters were introduced, ζ_b and ζ_c:

$$\zeta_b = \frac{M_{max}}{M_R},\ \zeta_c = \frac{M_{min}}{M_{max}} \tag{2.5}$$

where M_R is the maximum static moment capacity while M_{min} and M_{max} are respectively, minimum and maximum moment, of the specific load cycle. ζ_b represents the size of the cyclic loading while ζ_c represents the type of the cyclic loading. Note that $\zeta_c < 0$ means two ways cyclic loading. In the following these two loading parameters will be named load characteristics, as they represent the essential features of a load series.

One key issue of LeBlanc's research was to calculate dimensionless equations for scaling laboratory tests. This need relied on the fact that friction angle and shear stiffness found in laboratory significantly differ compared to those actual of full-scale tests. Such a difference is commonly attributed to the frictional behaviour of the sand that depends on the isotropic stress level which, of course, largely changes between small-scale and reality.

The most relevant non-dimensional relationship derived was between dimensionless moment $\tilde{M}$ and dimensionless rotation $\tilde{\theta}$:

$$\tilde{M} = \tilde{k}(\tilde{V}, \tilde{e}, \eta) \cdot \tilde{\theta} \tag{2.6}$$

where $\tilde{V}$ is the non-dimensional vertical load, $\tilde{e}$ is the non-dimensional eccentricity, η is the slenderness ratio, and $\tilde{k}$ is the non-dimensional stiffness. Equation (2.6) stated that: once the relationship between non-dimensional moment and non-dimensional rotation (at constant $\tilde{V}, \tilde{e}$ and η) is gained in small-scale tests, it can be applied on large-scale.

The results of the tests were evaluated by using non-dimensional parameters, e.g. the non-dimensional rotation:

$$\frac{\Delta\theta(N)}{\theta_s} = \frac{\theta_n - \theta_0}{\theta_s} \tag{2.7}$$

wherein the involved rotations are shown in Figure 2.3.

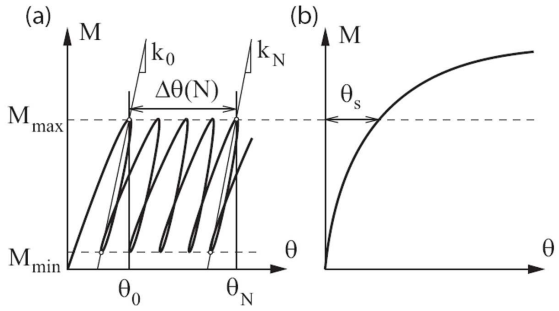

Figure 2.3: Cyclic and static test for rotation and stiffness. (LeBlanc *et al.*, 2010a).

The test programme carried out by LeBlanc *et al.* mostly investigated the changes in behaviour with respect to the initial density (I_D), applied load, and number of cycles.

A remarkable result obtained was an equation stating the accumulate displacement with respect to the number of cycles:

$$\frac{\Delta\theta(N)}{\theta_s} = T_b(\zeta_b, I_D)T_c(\zeta_c) \cdot N^{\alpha} \tag{2.8}$$

where T_b and T_c are dimensionless functions depending on relative density and loading characteristics (see LeBlanc *et al.* (2010a) for detailed explanation). Equation (2.8) expresses the exponential behaviour of the non-dimensional rotation. In a similar manner also a relationship for stiffness depending, again, on number of cycles and load characteristics was found. Some other specific results were pointed out. For instance, the most burdensome load condition was found at load characteristic $\zeta_c = -0.6$ as shown in Figure 2.4.

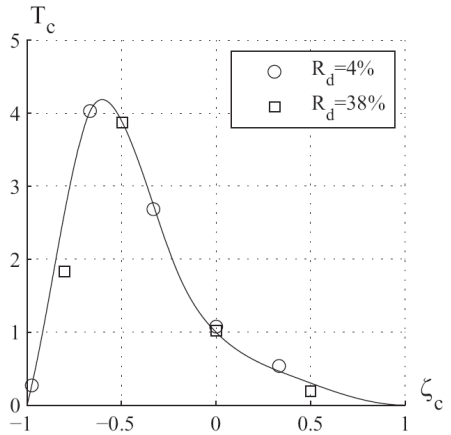

Figure 2.4: ζ_c against T_c, R_d is the relative density. (LeBlanc *et al.*, 2010a).

Lately a comparison was made between DSM and the LeBlanc's approach. Results regarding the accumulated displacement were found similar both quantitatively and qualitatively (Achmus *et al.* , 2010).

Random Cyclic Loading

LeBlanc *et al.* (2010b) assessed the accumulated rotation of a stiff pile due to a random cyclic loading. The method was based on the previously presented article, whereby a prediction of stiff pile behaviour under cyclic loading was given. Laboratory tests were carried out by means of the same cyclic loading rig.

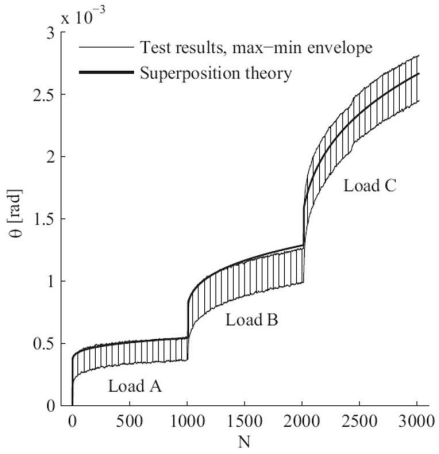

Figure 2.5: Test result and prediction compared. LeBlanc *et al.* (2010b).

Firstly the accumulated rotation was assumed, and demonstrated to be, independent of the load sequence. Thereafter, a strain superposition rule was presented, and in turn confirmed by experiments cf. Figure 2.5. The reversal load effect was addressed by simply subtracting the number of reversal cycles, where the load reversals was found by applying a rainflow-counting procedure on time-series of varying loads. Finally, a design chart for stiff piles subjected to two ways random loading was achieved. The overall method entirely relies on the empirical parameters previously presented such as T_c and T_b. Therefore, to prove its reliability further research should be focused on finding the dependence of such parameters with high accuracy.

Peralta's Approach

Peralta (2010) conducted 1-g tests on both, rigid and flexible piles, under horizontal cyclic loading. The piles were driven in dry sand. A first problem was to find reliable scaling laws whereby quantitative interpretation of tests could be used for real-scale prototypes. This issue was accomplished by proposing a valid similitude law through which results of small-scale tests could be applied on real-scale prototypes. The dimensionless pile displacement was expressed as:

$$\frac{y_N}{L} = f_h \cdot f_{EI} \cdot f_d \cdot f_H \cdot f_n \cdot f_N \cdot \tag{2.9}$$

where every f represents a function for force eccentricity h, flexibility EI, diameter d, load H, porosity n, and number of load cycles N, respectively. Corresponding functions for most of the variables involved were found in literature. For instance, the static force-displacement relationship, was assessed by the power law which states that the displacement is proportional to a power of the horizontal load. Thus, the dimensionless displacement was expressed as:

$$\frac{y}{L} = \left(\frac{H}{\gamma \cdot L^3}\right)^{\alpha} \cdot C \tag{2.10}$$

where C is a constant depending on pile geometry and soil property, and α is an exponent that was found varying between rigid, and flexible piles. Relationships such as equation (2.10) were ascribed to all Π-products presented in equation (2.9). The final result was an equation capable of describing the non-dimensional displacement $\frac{y_N}{L}$ of a pile. Thereafter, an example of calculation for a real pile loaded by a storm loading was given. Further, a comparison with the current method for accounting cyclic loading of the standard API (2002) was presented. A drastic deviation between the two methods was pointed out regarding rigid piles.

Another interesting result regarded the accumulated displacement of the same piles under different load paths. The accumulated displacements resulted, to a certain extent, dependent on the load path, in contrary to what LeBlanc *et al.* (2010b) assumed and demonstrated in the previous reported article.

Cyclic Tests on Suction Caissons

By the knowledge of the author only a few papers have investigated the dynamic behaviour of suction caissons. One of them was written by Zhu *et*

al. (2010). The whole concept was to a large extend similar to that adopted by LeBlanc *et al.* (2010a). The loading characteristics ζ_c and ζ_b and also the dimensionless ratio for accumulated rotation $(\theta_n - \theta_0)/\theta_s$ were taken from LeBlanc's studies. The non-dimensional relationships were achieved by carrying out a dimensional analysis on caisson foundations cf. Kelly *et al.* (2006a). The cyclic loading rig was basically the same, of course it was properly adapted to the new kind of foundation. The bucket was installed by pushing. Initially monotonic tests were conducted in order to determine the ultimate bearing capacity for different eccentricities. By the results of static tests a yield envelope was determined which was essential for calculating the cyclic load characteristic ζ_b cf. Figure 2.6.

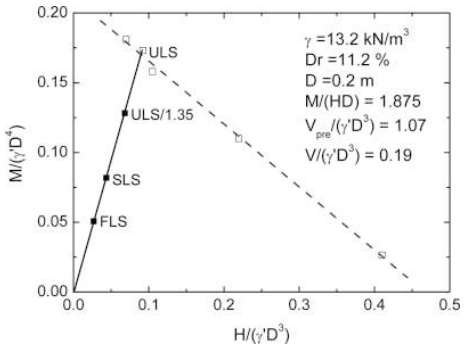

Figure 2.6: Monotonic moment capacity. (Zhu *et al.*, 2010).

Experimental data, gained from laboratory tests, gave a first prediction of accumulated rotation. Other considerations were made regarding the instantaneous centre of rotation and the unloading stiffness. The angular rotation was found to be linear with the number of cycles in logarithmic coordinates. Instantaneous centres of rotation in case of cyclic loading were located always at a greater distance that those of the static loading. Finally the normalized unloading stiffness was plotted against non-dimensional angular rotation. Depending on the ζ_b changes in stiffness were found. However, at fixed load characteristics the normalized unloading stiffness remained constant.

An overview on the cyclic loading studies review presented above is illustrated in Figure 2.7.

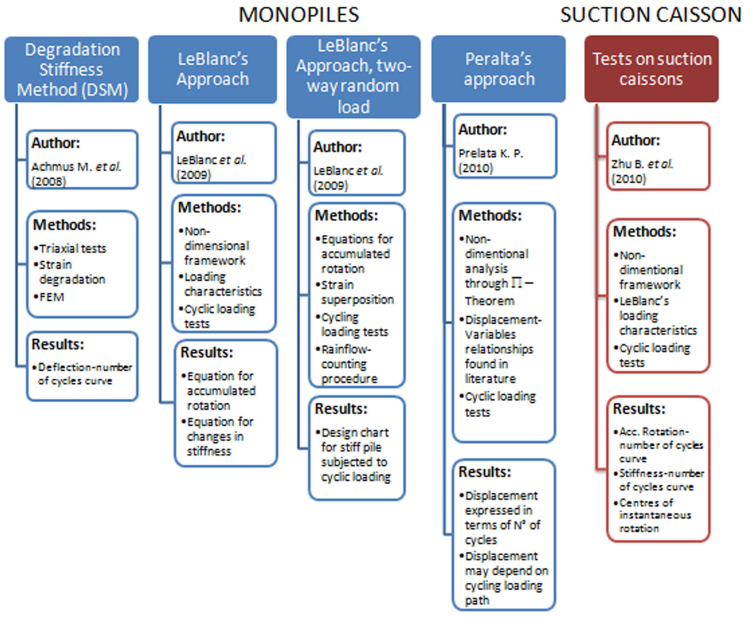

Figure 2.7: Overview on cyclic loading studies

Chapter 3

Dimensional Analysis, π-Theorem

The dimensional analysis is a method which allows for finding the dependency on physic and geometric parameters, of a certain phenomenon, on the base of dimensional homogeneity. The advantages of the dimensional analysis are:

- simpler relationships, less number of parameters;
- relationships obtained are more general, possibility of establishing similitude criteria ;
- possibility of carrying out experiments in small-scale and apply results on large-scale;
- rough estimation of the parameters importance, if a parameter is small it does not influence much the phenomena.

The first step of the analysis is the well known π-Theorem. In the following a general explanation of the theorem and its specific application for this thesis are given.

3.1 Statement and Hypotheses

In developing a dimensional analysis fundamental dimensions, variables and π-groups of a given problem must be introduced. The fundamental dimensions (or primary dimensions) are simply the physic fundamental dimensions involved in the problem (for instance length, force, time). By definition their combinations form any variable of the problem. π-groups are dimensionless monomials composed by a product of the variables involved in the original problem.

The π-Theorem states that: if a problem is described by a dimensionally homogeneous equation, such equation can be reduced to a relationship among a complete set of dimensionless products (Langhaar, 1951).

A relationship is said to be dimensional homogeneous if it is independent of fundamental units of measurement.

In practical terms, assuming that an unknown dimensionally homogeneous equation has k variables involved, the original equation can be rewritten by a relationship between k-r dimensionless groups. These groups are named π-groups, r, in most cases, is the number of fundamental dimensions in the problem.

In succinct mathematical form if the original equation is:

$$u_1 = f(u_2, u_3, ..., u_k) \tag{3.1}$$

after applying the π theorem Equation 3.1 can be rewritten as:

$$\pi 1 = g(\pi_2, \pi_3, ..., \pi_{k-r}) \tag{3.2}$$

In equation 3.1 every u_i is a variable involved in the problem whereas in equation 3.2 every π_i is a π-group formed. To create proper π-groups, a recurring set formed by a chosen series of variables u_i must be decided. In other words a recurring set is a group of variables forming all the dimensionless groups. The conditions to be taken into account during the execution of the method are listed below:

- every π-group must be uncoupled to any other group (independent of each other), so that no one group should be obtained combining together powers of other groups;
- each of the r primary dimensions must appear in at least one of the k parameters;
- a variable within the recurring set can not be chosen as a dimensionless group itself.

3.2 Specific Application

The practical problem developed in this thesis is the accumulated horizontal displacement of a bucket foundation under horizontal loading. To describe the force-displacement relationship, the variables considered as significant are: the vertical force V, the horizontal force H, the diameter of the bucket D, the length of the skirt d, the arm of the horizontal force calculated from the soil surface h, the friction angle φ, and the unit weight of the soil γ. All these variables are shown in the simplified system depicted in Figure 3.1.

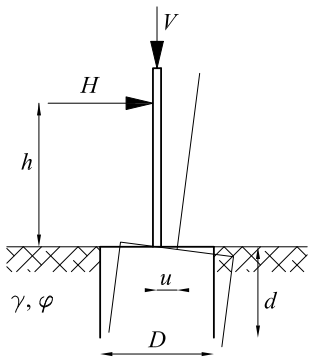

Figure 3.1: Variables involved in the dimensional analysis.

The original problem can be written as

$$u = f(H, h, V, d, D, \varphi, \gamma) \tag{3.3}$$

It is worth noticing that in writing Equation 3.3 the skirt has been assumed as entirely rigid. Among the significant variables there are two fundamental dimensions, namely force $[F]$ and length $[L]$. The variables, unit weight γ, and skirt length d, are chosen to form the recurring set. For γ dimensions are $[FL^{-3}]$ whilst for d[L] is the dimension. The fundamental dimensions can be rewritten as products of recurring set variables:

$$[L] = d \tag{3.4}$$

$$[F] = \gamma \cdot d^3 \tag{3.5}$$

The π-groups are thus formed by taking each of the remaining variables and making them non-dimensional. For instance the displacement y has dimension $[L]$, thereof the first π-group is straightforward

$$\pi_1 = \frac{y}{d} \tag{3.6}$$

The second π-group has the horizontal force H as object. H has dimension $[F]$. This means that $H \cdot F^{-1}$ is non-dimensional. In terms of variables:

$$\pi_2 = \frac{H}{\gamma \cdot d^3} \tag{3.7}$$

Stepwise, all the remaining variable must be taken into consideration and transformed into dimensionless groups. With these products in hand, Equation 3.3 becomes:

$$\frac{u}{d} = f\left(\frac{H}{\gamma \cdot d^3}, \frac{V}{\gamma \cdot d^3}, \frac{h}{d}, \frac{D}{d}, \varphi\right) \tag{3.8}$$

Note that φ was already dimensionless, and such it remains after applying the theorem.

Chapter 4

Similitude Theory

This chapter is aimed at finding, through theory and small-scale tests, consistent relationships to be employed in the design of bucket foundations. The study is relevant to the design of offshore wind turbine foundations. A similitude theory, regarding the horizontal displacement of bucket foundations under horizontal load, is put forward. A constitutive law of the soil medium and a load-displacement relationship for the bucket foundation are derived theoretically. Triaxial tests of sand, and small-scale tests of bucket foundation, are respectively employed to corroborate the theory. Attention is given to the different behaviour shown during compressive and dilative phase of the soil. Some analogy between triaxial tests and tests of bucket foundations are pointed out. A power law is capable to represent the dimensionless horizontal load-displacement relationship. In accordance with the theory, the exponent of the power law slightly varies between tests with considerably different features. The non-dimensional moment-rotation relationship is represented by a power law as well. In spite some limitations, the approach is considered valid for forces not up to failure, and therefore, for fatigue design. The research may be considered as a preliminary study, for predicting the behaviour of bucket foundations under long term cyclic loading.

4.1 Introduction

Monopod bucket foundations have been diffusely studied in recent years as a possible option for offshore wind turbine foundations. Such foundation consists of an upturned bucket with diameter D and length of the skirt d, cf. Figure 4.1. The main loads acting on the structure are the horizontal forces from wind and waves. The unique characteristic of the bucket foundation is the relatively simple and not expensive installation procedure, which can be carried out avoiding the utilize of heavy vessels (LeBlanc, 2009). This study employs a theoretical approach and data from small-scale tests to predict the horizontal load-displacement curve of monopod bucket foundations.

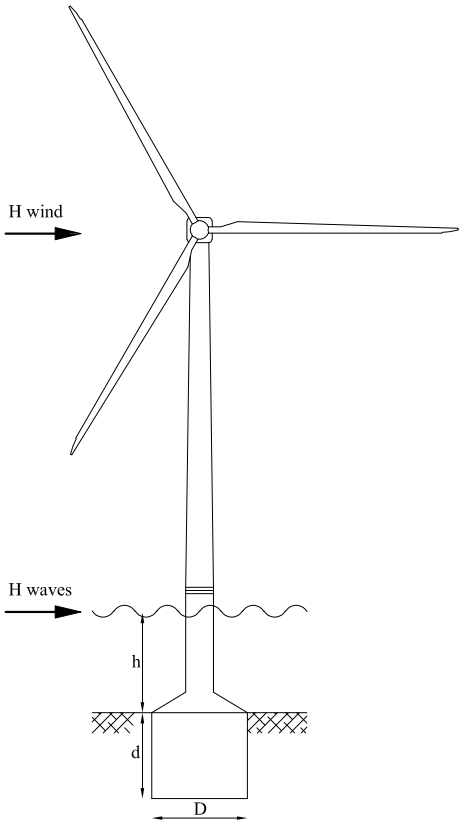

Figure 4.1: Wind turbine over mounted on a monopod bucket foundation. After LeBlanc (2009).

Dimensional analyses are essential when small-scale tests are accomplished within the field of geotechnical engineering. In fact, when an interface soil-structure is object of study, it is difficult to provide laws which are able to perfectly reproduce, in small-scale, the real-scale behaviour. In order to apply the results obtained with small-scale test to large-scale prototypes a similitude theory must be addressed. In this paper a similitude theory for bucket foundations is put forward stepwise. The behaviour under investigation is the horizontal displacement of a bucket foundation loaded by a horizontal force. The case of study is relevant for the design of offshore wind turbine foundations.

In the hope of obtaining a fully proven similitude theory three essential statements have been employed.

- A constitutive law for soil medium and a load displacement relationship for bucket foundations must be derived and expressed by means of

dimensionless variables only.

- The constitutive law and load displacement relationship must be analogous (Gudehus and Hettler, 1983).
- The constitutive law and load displacement relationship must be corroborated through small-scale tests.

For clarity's sake, it is worth saying that triaxial tests on dense sand, are used for proving (or disproving) the constitutive law, while small-scale tests of bucket foundations in dense sand, are adopted for proving the load-displacement relationship.

The first statement enables model and prototype to be comparable if, and only if, they are completely similar, i.e. non dimensional variables assume same values in the model and in the prototype (Langhaar, 1951). Complete similarity is normally possible only when geometric similarity exists between model and prototype. Besides, when soil is involved, its properties shall be equal in laboratory and in reality.

Furthermore, the skirt of the bucket will be assumed entirely rigid. Therefore, a constitutive law for the material of the bucket foundation does not concern our purpose. Further limitations and assumptions of the approach are stated in the following.

4.2 Constitutive Law

A constitutive law for cohesionless soil under cylindrical compression and extension was presented by Gudehus and Hettler (1983), on the base of a more general formulation given by Hettler (1981). In the first article the two authors expressed the constitutive law regardless of excess pore pressure and viscous effect. The constitutive law is theoretically derived in this section in the same manner as in the mentioned article.

Initially a monotonic stress path leads to the initial principal stresses: $\sigma_{0,1}$ and $\sigma_{0,2} = K_0 \cdot \sigma_{0,1}$ where K_0 is the coefficient of earth pressure at rest. Subsequently, an additional load (i.e. not up to the failure state), causes another stress path defined by $\Delta\sigma_1$ and $\Delta\sigma_2 = K \cdot \Delta\sigma_1$ where K is another earth pressure coefficient. The relative deformation results in the two principal directions which are $\Delta\varepsilon_1$ and $\Delta\varepsilon_2$. Now, in order to obtain a mathematical relationship between stress and strain states, a set of hypotheses (HP) will be stated. Since horizontal stresses and strains are relevant for this research,

in the following hypothesis only $\Delta\sigma_2$ and $\Delta\varepsilon_2$ will be considered. Of course, corresponding expression for $\Delta\sigma_1$ and $\Delta\varepsilon_1$ can be derived as well.

HP1: The stress-strain relationship can be expressed by means of solely dimensionless variables:

$$\Delta\varepsilon_2 = f_2\left(\frac{\Delta\sigma_2}{\sigma_{0,2}}, K, K_0\right) \tag{4.1}$$

As a result of that, f_2 can be seen as a function of non-dimensional products. As such, the first product $\Delta\sigma_2/\sigma_{0,2}$, should remain the same in small and large-scale, and more generally, under any confining pressure.

HP2: Applying the same stress path to a soil medium with different void ratio e, the strain path differs only by a factor C_e which depends on e.

HP3: By plotting on a log-log scale $\Delta\varepsilon_2$ vs $\Delta\sigma_2/\sigma_{0,2}$ a straight line must result. The slope of this line, μ, depends nor on e neither on K and K_0.

Naming $A\varepsilon_2$, the factors which depends on K and K_0, and considering the three hypotheses, it turns out that the corresponding function related to equation (4.1) can be written as a constitutive law

$$\Delta\varepsilon_2 = A\varepsilon_2 C_e\left(\frac{\Delta\sigma_2}{\sigma_{0,2}}\right)^{\mu} \tag{4.2}$$

Note that the slope μ in equation (4.2) is a constant of the soil.

4.3 Load-Displacement Equation

4.3.1 Original Form

The variables which play a significant role in the behaviour of a bucket foundation under horizontal static load are depicted in Figure 4.2.

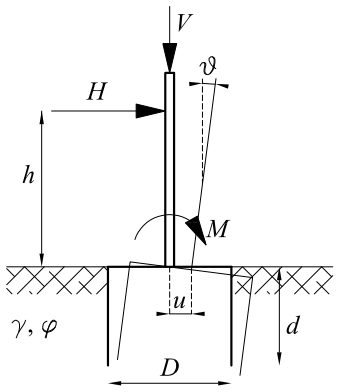

Figure 4.2: Significant variables taken into account in developing the dimensional analysis.

H and V are the horizontal and the vertical force, respectively, h is the arm of the horizontal force, d is the length of the skirt, D is the diameter of the bucket, φ the friction angle of the soil, γ the unit weight of the soil, and u the horizontal displacement of the foundation measured in the centre of the bucket at seabed level. Note that φ is a function of void ratio, e, and mean effective stress, p'.

When a bucket foundation is loaded by a horizontal force, its horizontal displacement can be expressed as

$$u = f_s\left(H, V, h, D, d, \gamma, \varphi\right) \tag{4.3}$$

where f_s is, as yet, an unknown function.

4.3.2 Dimensionless Form

For applying the dimensional analysis to a practical problem, a first necessary hypothesis to be employed is the dimensional homogeneity of the solving problem equation. Such a property characterizes an equation if that equation is independent of fundamental units of measurement (Langhaar, 1951). Hence, supposing equation (4.3) dimensionally homogeneous the Buckingham's Theorem (Buckingham, 1914) can be applied and, thereof, the original set of variables (equation (4.3)) is reduced to a dimensionless set

$$\frac{u}{d} = g_s\left(\frac{H}{\gamma d^3}, \frac{V}{\gamma d^3}, \frac{h}{d}, \frac{D}{d}, \varphi\right) \tag{4.4}$$

wherein g_s is the generic corresponding function that shall be found, in the first place theoretically and thereafter numerically by means of small-scale tests. More precisely a corresponding equation should be assessed for every dimensionless variable presented in equation (4.4), so that

$$\frac{u}{d} = g_H \cdot g_V \cdot g_h \cdot g_D \cdot g_\varphi \tag{4.5}$$

Evidently, equation (4.4) remains valid in small-scale as well as in large-scale only if the dimensionless variables of the model are equivalent to those of the prototype. In other words, dimensional similarity between model and prototype must exist.

It is important to point out that on the scalability of small-scale test results, relies the peculiar benefit of the dimensional analysis. On the other hand, thereby, the method becomes less general being based on a case by case analysis.

In addition, the application of Buckingham's Theorem should be proven by demonstrating that the set of dimensionless variables of equation (4.4) is a complete set. By definition a set of dimensionless variables (or dimensionless products) is complete if each of them is independent of the other (Langhaar, 1951). Thus, strictly speaking, every corresponding function should be addressed in order to have clear how it effects the behaviour. However, it will be shown that only one main function will be employed. All the other corresponding functions will be included in one parameter of the main function.

4.3.3 Power Law

The fundamental corresponding function for the static force-displacement relationship has been chosen as a power law. Such a law, which states that the lateral displacement of a rigid structure is proportional to a power of the horizontal load, was detailed demonstrated by Hettler (1981). Besides, in Gudehus and Hettler (1983) load-displacement relationships were derived for other kinds of rigid structures. However, the fundamental steps remained the same. Recently, the power law, has successfully been used by Peralta (2010) in a research regarding piles under cyclic loading. Below, a simplified demonstration of the power law is presented for a bucket foundation. Figure 4.3 depicts the system soil-structure on which the following demonstration relies.

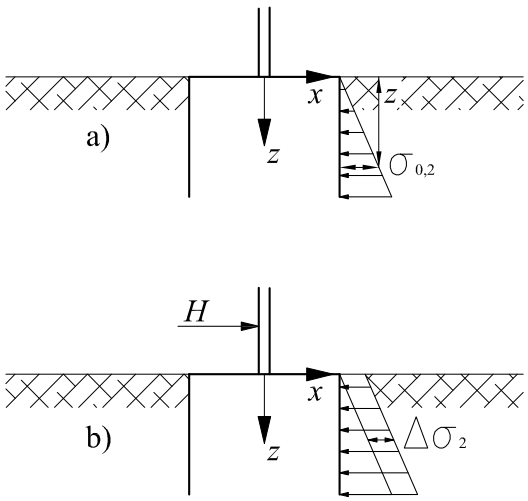

Figure 4.3: bucket foundation embedded in sand, subjected to horizontal load.

Before applying any load, cf. Figure 4.3 a), the soil is considered to be at the state of natural sedimentation, so that at a generic depth z the initial horizontal stress can be expressed as

$$\sigma_{0,2} = \gamma z K_0 \tag{4.6}$$

If a horizontal force H is applied, cf. Figure 4.3 b), to the bucket foundation, displacements on the x-z plane will occur. Taking the horizontal displacement, u, as main object of interest, its corresponding horizontal strain can be expressed by

$$\Delta\varepsilon_2 = k_\varepsilon \cdot \frac{u}{d} \tag{4.7}$$

where k_ε is a dimensionless factor dependent on the spatial coordinates. Substituting equation (4.6) and equation (4.7) into equation (4.2) gives

$$\Delta\sigma_2 = \gamma z K_0 \left(\frac{k_\varepsilon u}{A_{\varepsilon 2} C_e d} \right) \tag{4.8}$$

Now, assuming shear stresses along the skirt negligible for simplicity, the force H can be expressed by:

$$H = \int_0^d \int_{-D/2}^{D/2} \Delta\sigma_2 \mathrm{d}y \mathrm{d}z \tag{4.9}$$

In reality, considering a bucket foundation, the latter integral is not entirely correct. Indeed the effect of the curved skirt should be accounted into the integral. Although, according to the purpose of the demonstration, this thoroughness is negligible.

Hereafter, by substituting equation (4.8) in equation (4.9) the dimensionless horizontal displacement is obtained as

$$\begin{aligned} \frac{u}{d} &= \left(\frac{H}{\gamma}\right)^{\mu} \cdot \left(\iint zK_0 \cdot \right. \\ &\quad \left. \cdot \left(\frac{k_\varepsilon}{A_{\varepsilon 2} C_e}\right)^{1/\mu} \mathrm{d}x\mathrm{d}y \right)^{-\mu} \end{aligned} \tag{4.10}$$

Finally, naming the second product C and rearranging the whole equation in dimensionless quantities the expression becomes

$$\frac{u}{d} = \left(\frac{H}{\gamma \cdot d^3}\right)^{\mu} \cdot C \tag{4.11}$$

At least two observations about the above demonstration should be pointed out. Firstly, as one can notice constitutive law and load-displacement equation demonstrations, have the limitation that initially soils must be in the condition of soil at "rest". This means that the initial principal horizontal stress, $\sigma_{0,2}$, depends only on K_0. Such an assumption can be considered true in laboratory as well as in real scale.

Secondly, not every dimensionless variable considered in (4.4) appear in (4.11). The friction angle $\varphi(e, p')$, the ratio D/d, and the load $H/(\gamma \cdot d^3)$ are definitely well represented, whereas the arm, h/d, and the vertical force, $V/(\gamma \cdot d^3)$, do not take part in the demonstration. Nevertheless it is reasonable thinking that the coefficient C can be expressed by:

$$C = g_V \cdot g_h \cdot g_D \cdot g_\varphi \tag{4.12}$$

Such assumption will be proven by interpreting small-scale test result.

The load-displacement relationship obtained in this section seems to be analogous to the constitutive law derived in equation (4.2). Besides, both equations have been expressed in non-dimensional variables. Hence, two essential conditions of the similitude theory have been respected. Therefore equation (4.11) will be employed as the corresponding function for the load displacement behaviour of a bucket foundation. Consequently, equation (4.4) becomes

$$\frac{u}{d} = g_s = \left(\frac{H}{\gamma \cdot d^3}\right)^{\mu} \cdot C \tag{4.13}$$

4.4 Experimental Corroboration

Consolidated Drained-Triaxial Tests

In order to check the constitutive hypothesis, Hettler (1981) carried out particular triaxial tests to avoid non-uniform sample deformation and possible errors in the measurement. The Consolidated Drained (CD)-triaxial tests examined in this paper, are considered as sufficient reliable for the purpose aimed. All tests have been conducted by Ibsen*et al.* (1995) on Aalborg University sand No. 0. Note that Baskarp Sand No. 15 is equal to Aalborg University sand No 0. Test equipment and testing procedures, are presented in Ibsen (1999). The index properties of the sand are shown in Table 4.1.

Table 4.1: Index properties of Aalborg University sand No. 0. (Ibsen, 1999).

Property	Value	Unit
$d_{50} = 50\%$ - quantile	0.14	[mm]
$C_u = d_{60}/d_{10}$	1.78	[-]
Specific grain density d_s	2.64	[g/cm^3]
Maximum void ratio e_{max}	0.86	[-]
Minimum void ratio e_{min}	0.55	[-]

The interpretation of CD-triaxial tests is focused on samples with density index $I_D = 1.00$, as this is close to usual soil conditions at offshore sites at shallow depth (0-30 m). Figure 4.4 shows, in dimensionless form, the result of six drained triaxial compression tests performed with the same density index at different confining pressures σ_c. In contrary to what stated in *HP1*, these curves badly coincide.

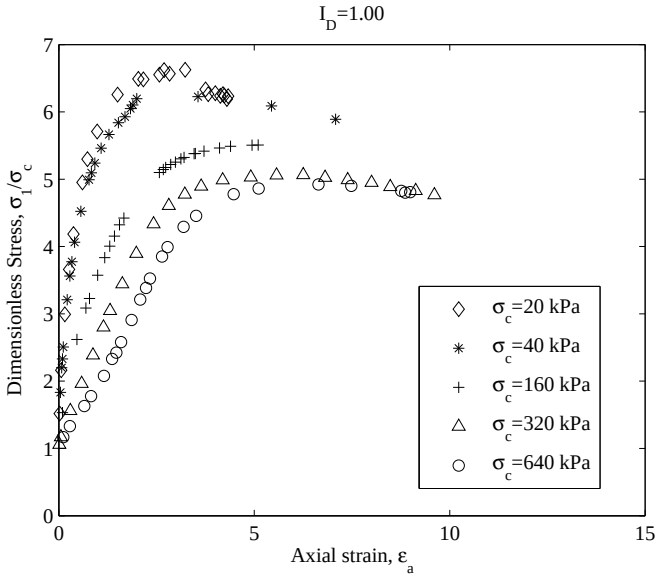

Figure 4.4: Dimensionless stress-strain behaviour in drained triaxial compression tests on sand with $I_D = 1.00$.

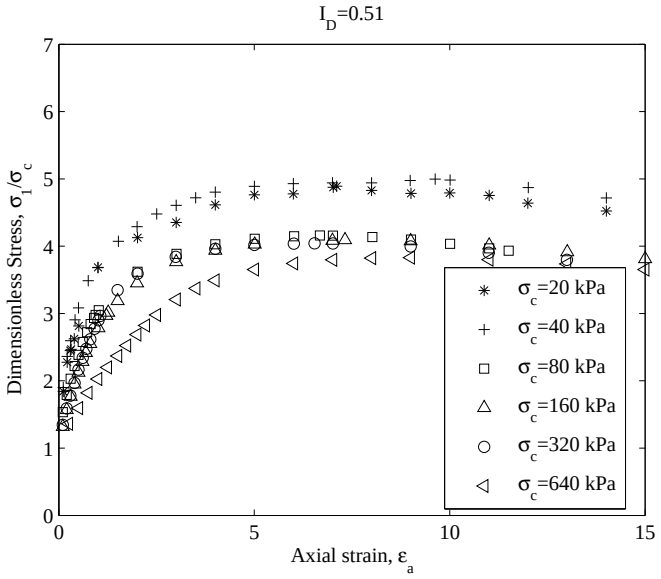

Figure 4.5: Dimensionless stress-strain behaviour in drained triaxial compression tests on sand with $I_D = 0.51$.

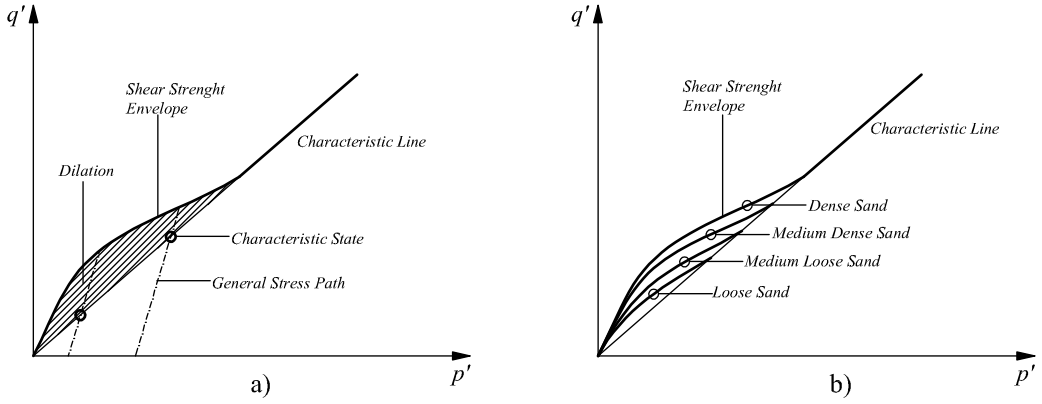

Figure 4.6: Typical Cambridge diagram for sand. After Ibsen (1999).

Thus, the stress-strain behaviour depends upon the confining stress. Nevertheless, this fact was expected and it can be attributed to the significant dilative behaviour presented by such a dense sand. Experiments on sand have shown that dilation occurs in dense sand and/or at low confining pressure (Ibsen, 1999). In Figure 4.6 is schematically illustrated the typical Cambridge diagram where the characteristic line and the shear strength envelope are depicted. The effect of the confining pressure at equal density index is emphasised by Figure 4.6a). Figure 4.6b) highlights how the shear strength depends on the sand density. It can be noted that the dilative behaviour is suppressed at high confining pressures, due to grain crushing. At those confining pressures the shear strength envelope comes to coincide with the characteristic line. For loose or medium loose sand the shear strength envelope remains close to the characteristic line, also at low confining pressures. As a confirmation of that, results on CD-triaxial tests on the same sand with $I_D = 0.51$ are shown in Figure 4.5. Note that the dependence of the stress strain behaviour on the confining stress is not as dominant as that in Figure 4.4. Particularly, the records $\sigma_c = 80$ kPa, $\sigma_c = 160$ kPa, and $\sigma_c = 320$ kPa of Figure 4.5, are rather similar. More remarkable results were obtained by Peralta (2010), who examined CD-triaxial tests on looser sand samples ($I_D = 0.40$). Peralta could fully corroborate the constitutive law by the results of those tests. More considerable results for the purpose of this paper, can be seen in Figure 4.7 where the same records of Figure 4.4 are plotted in a $(\Delta\sigma_1/\sigma_c)$-$\varepsilon_a$ plane on a double logarithmic scale.

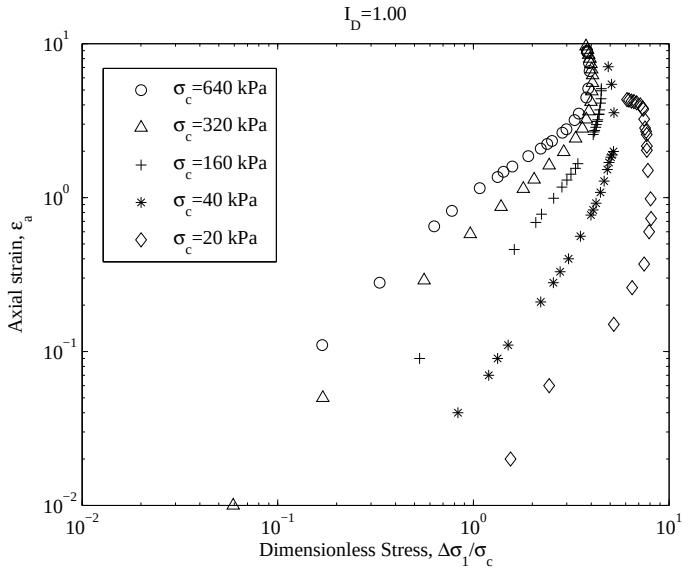

Figure 4.7: Dimensionless stress-strain behaviour in drained triaxial compression tests on dense sand.

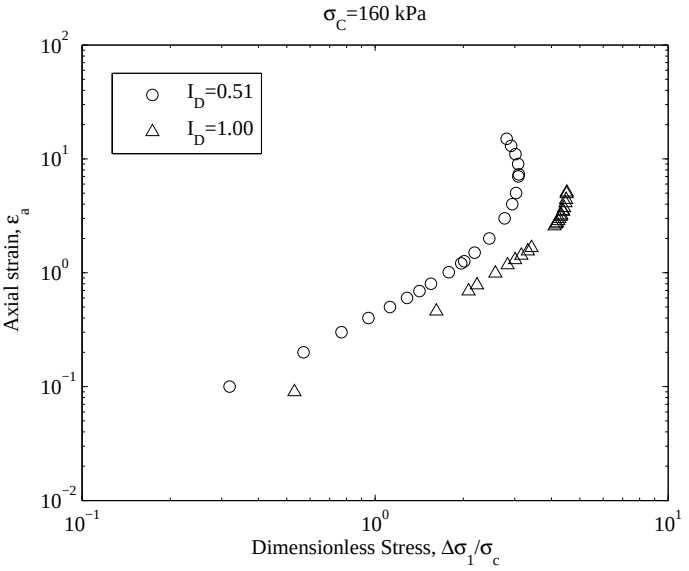

Figure 4.8: Comparison between CD-triaxial tests conducted on samples with different density index at the same confining pressure.

Figure 4.7 shows that every record collected follows a certain straight line until it begins to bend toward failure. For each confining pressure the point where the line shape changes was found to be correspondent to the charac-

teristic state. According to the definition given by Ibsen (1999) the characteristic state of the soil is the stress state at which $\delta\varepsilon_v/\delta\varepsilon_1 = 0$. In other words, before the Characteristic State the soil compresses, whereas after the Characteristic State the soil dilates. In Figure 4.7 the slope of the straight lines seems to be very similar among all the records. As a confirmation of that, fitting with a power law these straight lines, the exponent μ of equation (4.2) resulted to be only slightly variable with values ranging from 1.31 to 1.71. Note also that with decreasing confining stress each line is translated toward higher values of $\Delta\sigma_1/\sigma_c$. This fact can be attributed to the effect of the constitutive law coefficient $A\varepsilon_2(K, K_0)$. By the above considerations the constitutive law is partially corroborated. More support to the theory is provided by Figure 4.8 where, a typical comparison between records of test conducted at the same σ_c with different void ratios, is given. Also these data present the same slopes before the bending point. These records validate *HP2*. The conclusion which can be drawn is that the constitutive law (equation (4.2)) is consistent with triaxial tests data as long as soil dilation does not occur. As a direct consequence of that, the similitude theory is now limited only to the compressive states of the soil.

Tests on Bucket Foundations

Small-scale tests on bucket foundations were carried out by Larsen (2008) at the Geotechnical Laboratory at Aalborg University. According to the offshore soil conditions all tests were performed with a high density index ($I_D > 0.8$). For conducting the experiments 0.4 m, 0.3 m and 0.2 m bucket diameters were chosen. For each diameter four embedment ratios were adopted, d/D =0.25, 0.5, 0.75 and 1. In most of the tests the 0.3 m diameter bucket was adopted. In the following, results obtained by Larsen (2008) are presented, and evaluated, to fulfil the purpose of this paper. Some typical static test results are shown in Figure 4.9, where dimensionless displacement is plotted against dimensionless horizontal force on a double logarithmic scale. Note in the figure legend that foundation sizes, embedment ratios (d/D), vertical loads and heights of impact widely vary, from test to test. The density index nearly remains the same. Figure 4.9 shows that two distinct trends can be discerned from any of the records.

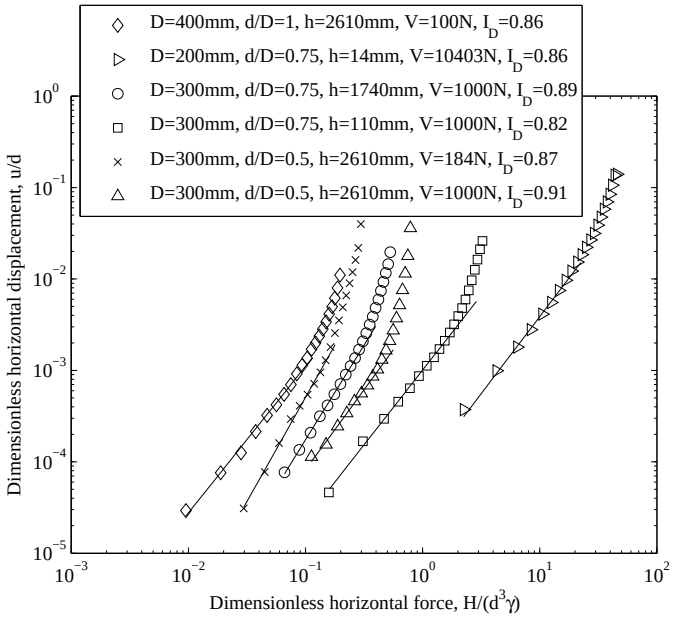

Figure 4.9: Dimensionless displacement as a function of dimensionless horizontal load for tests with different loading features.

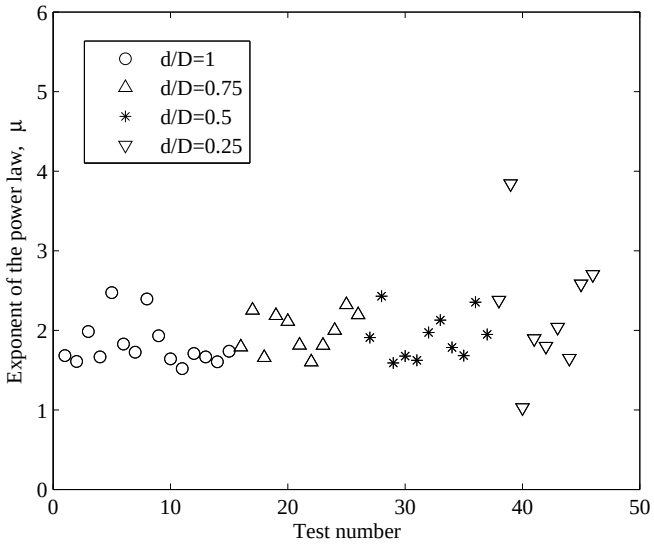

Figure 4.10: Exponent of the power law μ collected with four different embedment ratios.

The first part can be approximated with a straight line characterized by a

specific slope. Such line is emphasised by fitting with a power law the data recorded within 0.5 H_{max} (maximum horizontal force reached by tests), cf. Figure 4.9. At a certain point, after 0.5 H_{max}, the line ceases to be straight and tends to bend until failure occurs. The described tendency seems to be in analogy to what CD-triaxial tests previously showed. Hence, the curvature of the lines might refer to dilative states of the sand. Now, considering only the straight lines, a similar slope among all records can be observed. In Figure 4.10 the value of μ (exponent of the power law), calculated for 46 tests, is shown collected with the four different embedment ratios used. In spite a certain scatter, most of the exponents were assessed in the range of 1.6 and 2. Between the maximum and the minimum value a 34% difference was found. This was considered as acceptable, even thinking that the mentioned scatter was by no means related to the test typology. The variability of μ is, therefore, utterly attributed to the test sensitivity. Conversely, in tests carried out with buckets having $d/D = 0.25$, μ significantly changes. This can be ascribed to the different failure mechanism that concerns bucket foundation with $d/D < 0.50$. This limitation can be seen in Figure 4.11 where records of tests conducted with same load conditions, same diameter, and different embedment ratios are shown.

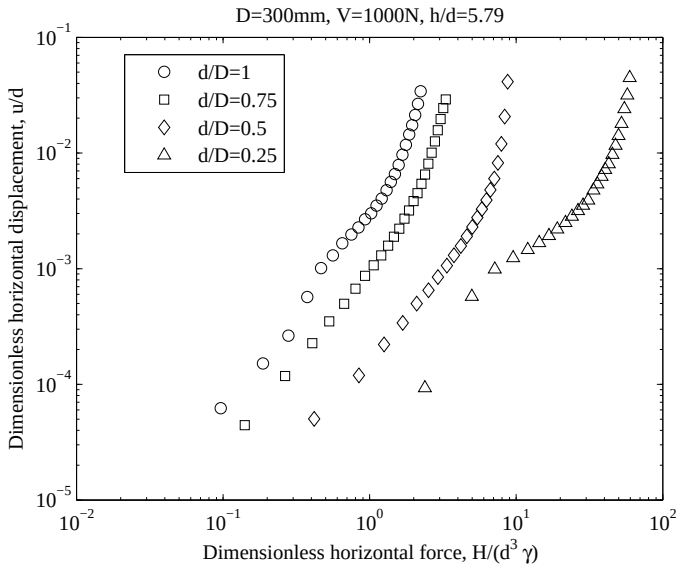

Figure 4.11: Records concerning buckets with same diameter, same loading condition and different embedment ratio.

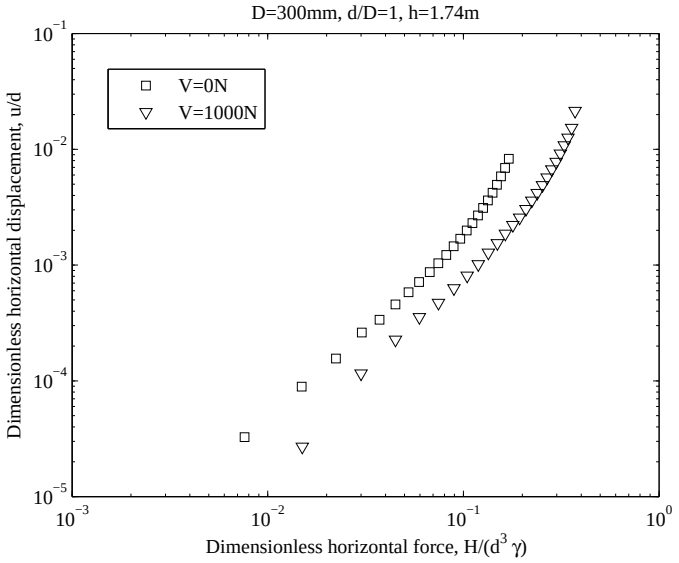

Figure 4.12: Comparison between two tests carried at the same conditions with only different vertical load.

Hence, regardless of buckets with $d/D = 0.25$ the first part of the records follows what was predicted by equation (4.11). The tendency is characterized by a nearly constant exponent μ and a coefficient C that depends on $\varphi(e, p')$, D/d, h/d and $V/(\gamma \cdot d^3)$. The influence of these dimensionless variables, except for $\varphi(e, p')$, was proven by comparing C of tests in which only one of the variable changed. As an example in Figure 4.12 are depicted two records obtained by tests in which only the vertical load differs. Note that the two records show the same slope, and that the record with $V = 1000$ N is shifted to the right. Therefore, fitting the data with equation (4.13) only the coefficient C changes. The friction angle $\varphi(e, p')$ could not be properly isolated because e and p' did not significantly change from test to test.

What stated above provides a satisfactory partial verification of the load-displacement relationship (equation (4.11)), and thereby corroborates the three previously employed hypotheses and the constitutive law itself. Briefly, for buckets having $d/D \geq 0.50$, loaded by a horizontal force within 0.5 H_{max}, the load-displacement equation well fits the small-scale tests data. Consequently, taking into consideration all the stated limitations, once the load-displacement relationship of a bucket foundation with specific features has been assessed through a series of small-scale tests, such equation may be used for predicting the displacement of a large-scale prototype.

Turning to the relationship between overturning moment and rotation, sim-

ilarly to equation (4.3) the rotation of the bucket, θ, can be obtained as

$$\theta = f_s\left(M, V, D, d, \gamma, \varphi\right) \tag{4.14}$$

Hence, employing the Buckingham's Theorem (Buckingham, 1914) the bucket rotation can be expressed by

$$\theta = g_s\left(\frac{M}{\gamma d^4}, \frac{V}{\gamma d^3}, \frac{D}{d}, \varphi\right) \tag{4.15}$$

Now, figure 4.13 shows typical trends of the horizontal displacement, u, against the rotation, θ. These records reveal a key feature of every test, which is the linear relationship between u and θ. This suggests that, the moment-rotation curves should have similar distribution to those of the horizontal load-displacement. Figure 4.14 depicts the dimensionless moment-rotation curve for four tests with different characteristics, on a double logarithmic scale.

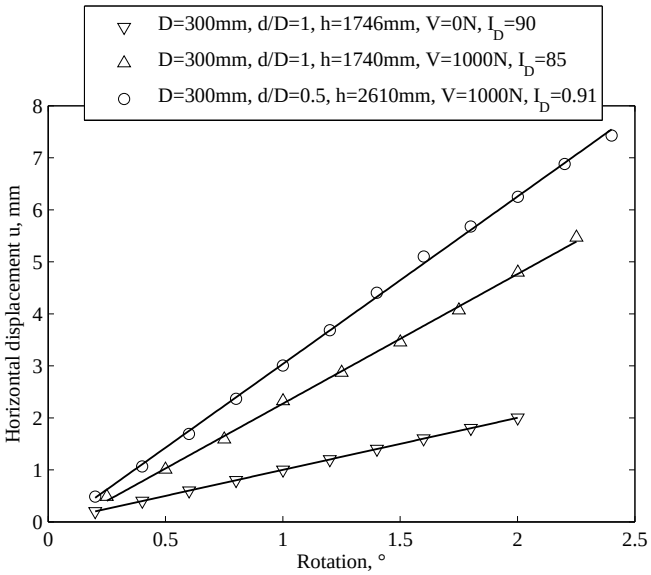

Figure 4.13: Horizontal displacement, u, as collected with the rotation θ.

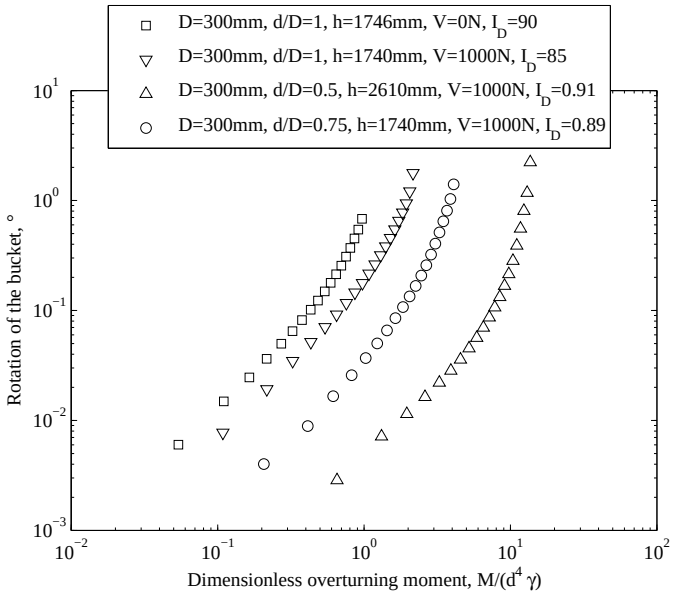

Figure 4.14: Rotation as a function of dimensionless overturning moment for tests with different loading features.

In fact, it is clear that the trend is similar to that found for the load-displacement curves. The power law capable to represent the straight part of the dimensionless moment-rotation records has the form

$$\theta = \left(\frac{M}{\gamma \cdot d^4}\right)^{\mu} \cdot C \tag{4.16}$$

As it was set out for the load-displacement case, the power law is no longer valid when $M > 0.5M_{max}$. The validity of equation 4.16, for forces not up to failure, might have significant consequences on the fatigue design. However, to enhance the reliability of the results, further research is necessary.

4.5 Conclusions

This paper introduces a similitude theory for bucket foundations in dense sand under static horizontal load. The main aim of the study was to assess a load-displacement relationship capable of properly representing the behaviour of such foundation in real-scale. The theory is based on previous similar researches conducted on piles. In order to have a fully proven theory

three conditions were initially employed. All of them were, to some extend, fulfilled.

A dimensionless constitutive law for sand was derived assuming three fundamental hypotheses. Consolidated drained-triaxial tests were examined in order to corroborate the assumptions. The experiments could not entirely confirm the three hypothesis. This was attributed to the dilative behaviour of dense sand. The constitutive law itself, was partially corroborated. Limit of its validity was deduced to be the compressive states of the soil.

By virtue of the constitutive law a non-dimensional load-displacement relationship was derived in form of a power law. Static test results of bucket foundations under horizontal load were examined to prove the theory. In analogy to what found for the constitutive law, also the load-displacement relationship could not be utterly corroborated. Record from tests on bucket with $d/D = 0.25$ did not confirm the theory. This was attributed to a different failure mechanism. Moreover, the power law matched with tests data only until a specific value of the horizontal load. The reason for this might be the turnabout from compressive to dilative state of the soil. Also the non dimensional moment-rotation curves were found to be well represented by a power law (thought with the same limitation of the load-displacement case). In spite these limitations, the theory was considered acceptable for forces not up to failure, and therefore, useful for fatigue design.

An additional limitation on the approach is the complete similarity between model and prototype. Such similarity is complete only when all the dimensionless products of the load-displacement relationship have the same value in the model as in the prototype.

A similar research regarding large-scale monopod bucket foundations should be conducted to confirm the findings of this paper. Besides, further studies should be focused on better investigation of the corresponding functions that have not been decoupled in this paper. Especially, a study concerning $\varphi(e, p')$ should be carried out by recreating the real-scale overburden pressure condition in laboratory, and thus, assess how C, and μ are affected by φ. Also the changing point, between compressive and dilative behaviour, shown by the record of small-scale tests, should be more profoundly investigated.

This study may be considered as an initial source for further research on long term cyclic loading of bucket foundations. The approach is not meant for forces up to the failure state.

Chapter 5

Laboratory Tests

In this appendix all devices, operations and methods that have been necessary to perform small-scale experiments on caisson foundations at the geotechnical laboratory at Aalborg University are described. Most of the data analysed in this thesis were obtained by Larsen (2008). On particular purpose for this thesis six additional experiments were conducted. The behaviour of the bucket foundation at different effective stress of the soil was investigated. The test program is listed in Table 5.1.

Table 5.1: Test program.

Test No.	Applied Overburden Pressure [kPa]
1	0
2	0
3	15
4	30
5	20
6	10

Throughout this Appendix all the procedures involved in conducting the test series of Table 5.1 are presented. The overall testing procedure slightly differs from that employed by Larsen (2008). The sand used for all tests was Aalborg University Sand No. 0. All details regarding such sand are set out in Appendix 6.2.

5.1 Preparation of the Test Box

A steel box, inner width 1600 mm x 1600 mm and inner depth 1150 mm was used as soil container, cf. Figure 5.1. The box was equipped with a drainage system on its bottom. The drainage system consisted of perforated pipes, 100 mm of draining material (gravel), and a sheet of geotextile. The perforated pipes were distributed in order to provide an equal drainage condition to the entire area. The geotextile sheet was needed for keeping the drainage

material clear of sand grains which could potentially occlude the drainage system.

The homogeneity of the soil from one test to another was required. This enabled the results obtained in different tests to be fairly comparable. In order to provide equal soil conditions, appropriate procedures were conducted in the preliminary phase of every test. In the following the soil preparation procedure is described.

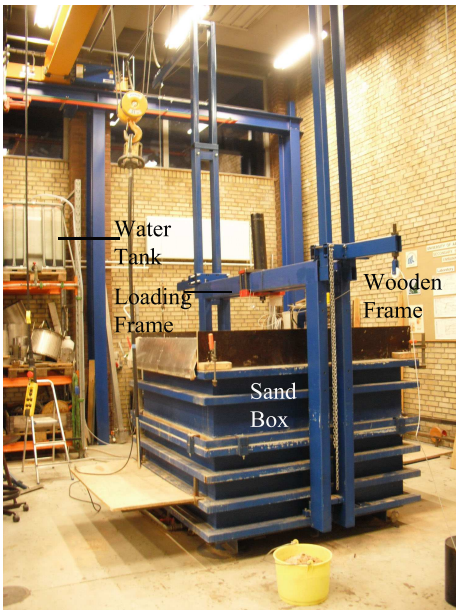

Figure 5.1: Suction caisson test rig.

5.1.1 Preparation Procedure

Through the drainage system the water level was raised on purpose of loosening up the sand. The water pressure gradient applied was kept under control through a transparent tube, and regulated by a valve situated on the inlet pipe. The water was provided by a water tank placed higher than the soil surface, cf. Figure 5.1. A wooden frame was placed on the sand layer to retain water and soil due to the loosening. Once the soil reached the complete saturation, the compaction could commence. In order to carry out a uniform compaction, a wooden plate with 64 holes was placed on the wooden frame. The entire area was, thereby, equally divided. The compaction was performed with a rod vibrator, by penetrating every hole in a systematic manner. In pulling back the rod vibrator the same velocity of the downward

way was to be kept. The sand compaction equipment is illustrated in Figure 5.2. The above procedure was repeated two times before the first test, and only one time before every subsequent test.

Figure 5.2: Wooden plate and rod vibrator.

Figure 5.3: Soil alignment operation.

During all the described operations no air had to enter the box through the drainage system. Therefore, the water level in the box was at any time kept above the drainage layer. At soil vibration concluded the alignment operation could be carried out and the water table was adjusted to the sand surface, cf. Figure 5.3. To reach the complete saturation, some water was slowly poured from above to avoid eventual sand loosening. Applying the

above described method ensured sand features, such as density, to have an acceptable deviation from test to test.

To ensure homogeneity of soil parameters a cone penetration test was utilized. A detailed explanation of the cone penetration test procedure is given in Section 6.2. A saturated soil was necessary in order to perform cone penetration tests and to vibrate the soil. However, not all tests were conducted with saturated sand. When suction was applied the sand was brought to the dry condition, cf. Section 5.2.2.

5.2 Testing Procedure

The six tests were carried out with a 300 mm diameterbucket foundation with embedment ratio equal to 1. The foundation is illustrated in Figure 5.4. No vertical load, exceeding the structure self weight, was added.

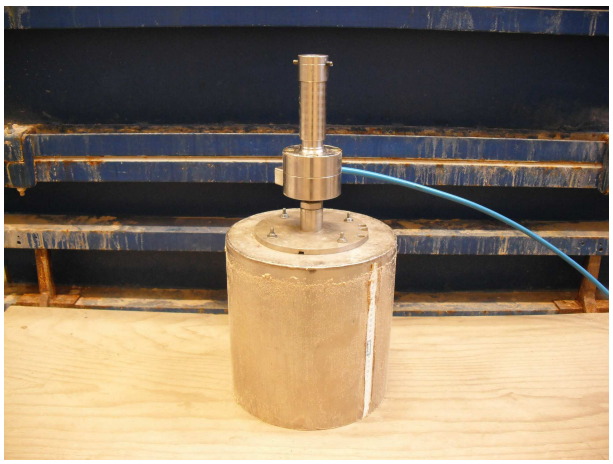

Figure 5.4: 300 mm diameter bucket.

A loading frame mounted on the sand box and fixed at the edges of it, cf. Figure 5.1, was necessary to perform all the operations. A PC-based data acquisition, HBM SPIDER 8, was used to transfer data from the measurement devices to the computer. Three phases were necessary to run a test: installation, suction application (when wanted), and loading action.

5.2.1 Installation of the Bucket Foundation

An electric motor mounted on the loading frame, forced the foundation into the soil. On the bucket lid three air outlet were located and kept in open position during the penetration. To avoid overpressure inside the bucket the penetration velocity was very low, approximately 80 mm/h. Once the lid had reached the soil surface, the air outlets were closed and the installation rig was delicately dismantled.

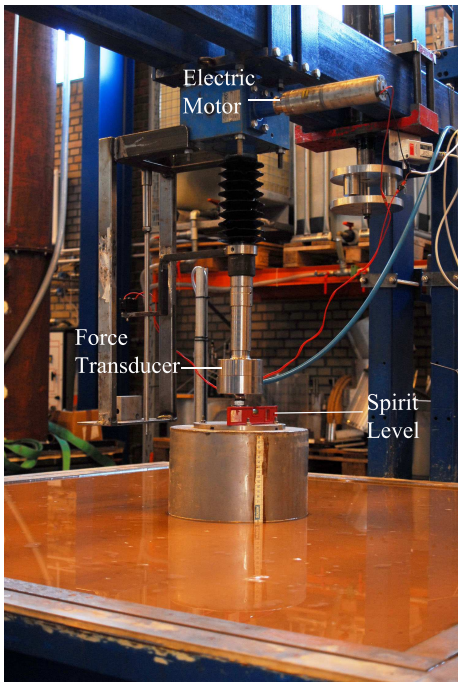

Figure 5.5: Installation rig.

The installation was monitored by using a force transducer placed between the bucket and the installation rig. The tilt of the bucket during installation was controlled by using a spirit level. A typical curve, depth-penetration force, is depicted in Figure 5.6. The installation rig is depicted in Figure 5.5.

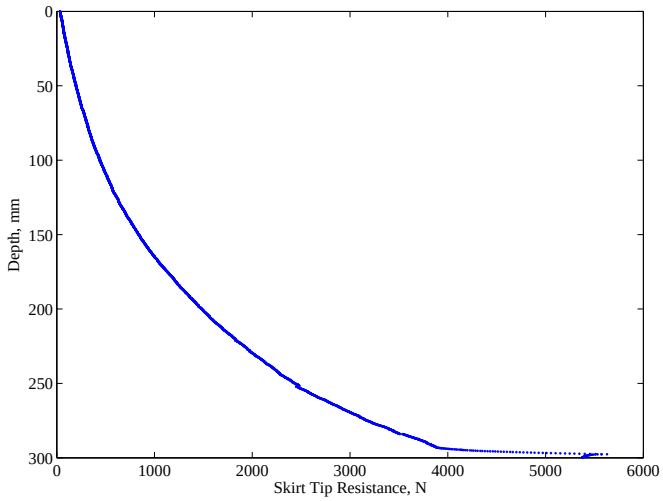

Figure 5.6: Penetration force against depth during bucket installation.

5.2.2 Effective Stress Increase

The most relevant innovation regarding the six novel tests was the utilize of a suction system to apply an exceeding overburden pressure to the soil surface, cf. Figure 5.7 and Figure 5.8.

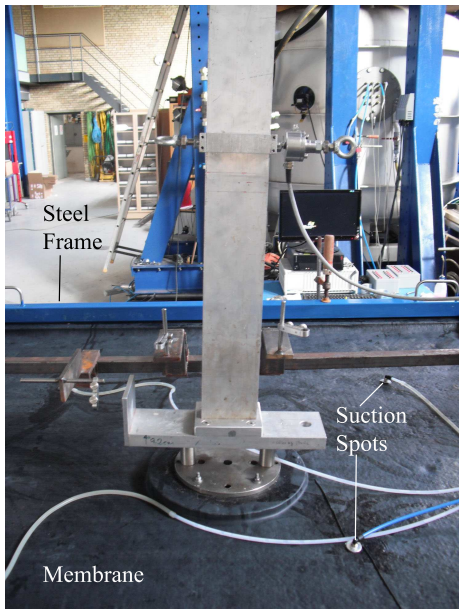

Figure 5.7: Membrane and suction spots.

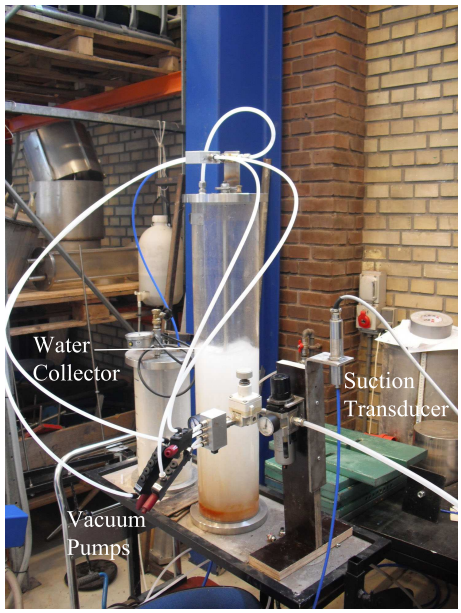

Figure 5.8: Suction system.

The suction system consisted of a membrane with four suction spots, each of them connected to a vacuum pump through a suction hose. The membrane was placed beneath the soil surface and fixed to the sand box edges by means of a steel frame and clamps. Between membrane and steel frame a washer was inserted in order to avoid leaks of air. Furthermore, between sand and membrane a filter was put to prevent eventual sucking of sand grains. An additional spot was placed on the membrane and connected to the data acquisition device by means of a pressure transducer of the type HPM P6A. The pressure was regulated with a control valve and kept steady during each test. The four vacuum pumps applied the suction through a sealed glassed cylinder to collect the water that unavoidably came out from the box together with air, cf. Figure 5.8. As a result of that, for all tests with suction applied, i.e. with increased effective stress, the soil was not in saturated condition.

5.2.3 Loading Phase

Once the bucket was installed and the measurement system set, the application of the horizontal quasi-static load could commence. A vertical bar, bolted on the lid of the bucket, was subjected to a horizontal force induced by an electric motor. The horizontal loading rig was mounted on the loading frame. The loading velocity was approximately 0.01 mm/s. The bucket foundation under horizontal load is shown in Figure 5.9.

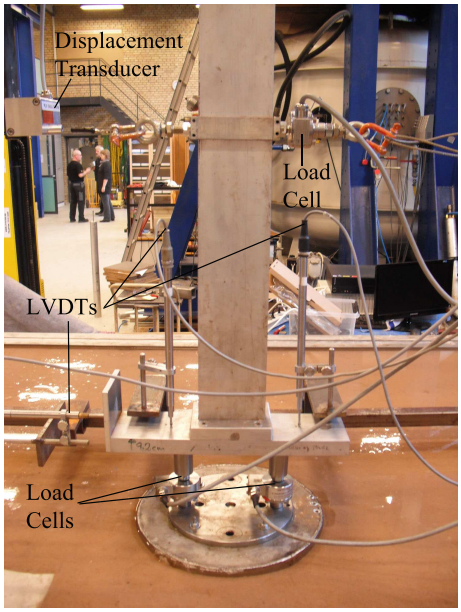

Figure 5.9: Bucket foundation during loading phase without overburden pressure.

For all tests the arm of the horizontal load was 600 mm. The moment-rotation curve for test no. 1 and test no. 6 are shown in Figure 5.10. Every test was conducted until failure of the soil occurred. When the effective stress was increased the failure was reached at much higher value of both applied moment and rotation. From Figure 5.10, it can be observed that the moment-rotation gradient ceases to increase significantly after 2° of rotation for Test no. 6 and after 1° of rotation for Test no. 1. The tests with suction applied were also subjected to an unloading-reloading phase.

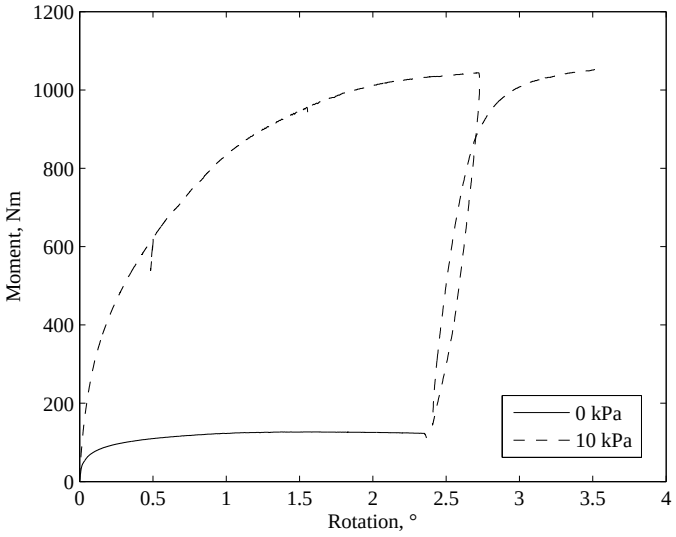

Figure 5.10: Moment against rotation for test no. 1 and test no. 6.

5.3 Deformations Measurement

The displacement of the bucket was measured by means of two perpendicular plates, on which three linear variable differential transducers (LVDTs) were placed. Two transducers, type HBM W20TK were located vertically and another, type HBM WA/50 was located horizontally. The measurements themselves, assessed during tests, did not provide the actual displacement of the foundation straightforward. In fact, some calculations were employed to figure the bucket displacement. The calculation process was based on that proposed by Larsen and Ibsen (2006). The system is depicted in Figure 5.11 and a picture is given in Figure 5.12.

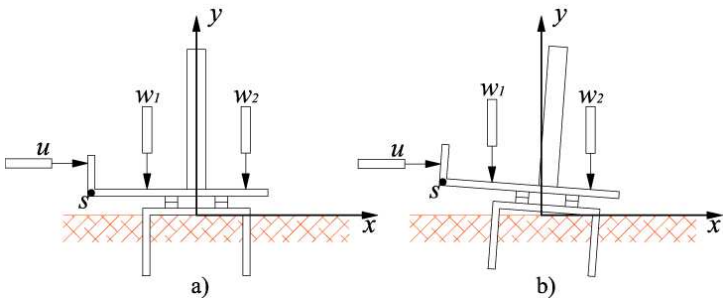

Figure 5.11: Initial and displaced configuration of the bucket with LVDTs. After Larsen and Ibsen (2006).

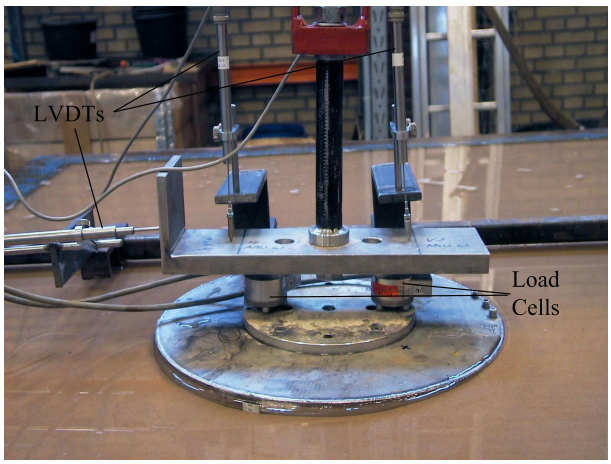

Figure 5.12: LVDTs and load cells. (Larsen, 2008).

The calculation for the displacement of the bucket begins with stating the coordinates of the LVDTs at both initial and deformed configuration. Below the coordinates are specified with respect to the origin of the system which is located on the bottom of the bucket lid as shown in Fig. 5.11. The coordinates, at the beginning of the experiment, can be expressed as:

$$u_{1,i} = (-185mm, 120mm);$$

$$w_{1,i} = (-100mm, 95mm);$$

$$w_{2,i} = (100mm, 95mm);$$

where u_1 refers to the horizontal displacement transducer, w_1 refers to the first vertical displacement transducer, and w_2 refers to the second vertical displacement transducer. When the displacement occurred the coordinates become:

$$u_{1,d} = (-185mm + \Delta x, 120mm);$$

$$w_{1,d} = (-100mm, 95mm + \Delta y1);$$

$$w_{2,d} = (100mm, 95mm + \Delta y2);$$

where Δx is the horizontal transducer measurement, $\Delta y1$ is the first vertical transducer measurement and $\Delta y2$ is the second vertical transducer measurement. The subscripts i and d refer respectively to the initial and displaced position.

The sign convention employed to measure vertical displacement w, horizontal displacement u, rotation θ and loads was chosen according to the one proposed by Butterfield *et al.* (1997). Note that any transducer measurement can be either positive or negative, depending on the displacement induced. For instance, according to the system illustrated on Figure 5.11, the second vertical measurement $\Delta y2$ is negative, while the horizontal measurement Δx is positive as well as the first vertical one $\Delta y1$.

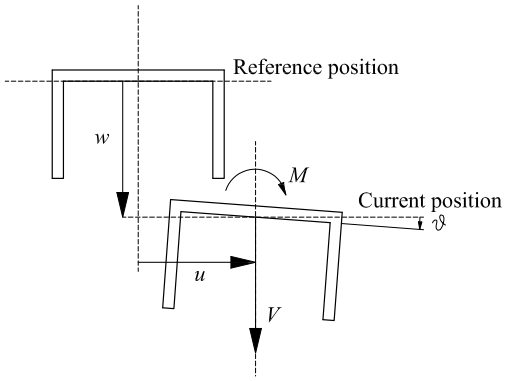

Figure 5.13: Sign convention for loads and displacements.After Butterfield *et al.* (1997).

The displacements of the bucket, u and w were measured by representing the perpendicular plates with two lines, cf. Figure 5.14. These two lines, l_1 and l_2, can be expressed with two linear equations:

$$l_1 : \; y = a_1 \cdot x + b_1 \tag{5.1}$$

$$l_2 : \; y = a_2 \cdot x + b_2 \tag{5.2}$$

where angular coefficients a_1 and a_2 and constants b_1 and b_2 were deduced for every test by elaborating the transducer coordinates and transducer measurements following equations (5.3)-(5.6). Figure 5.14 shows the two perpendicular plates in the displaced configuration. In the same figure the junction

of the two plates s, the midpoint m of line l_1 and the points of the transducer measurements u_d, $w_{1,d}$ and $w_{2,d}$ are illustrated as well.

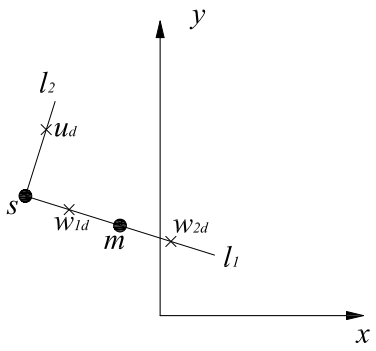

Figure 5.14: l_1 and l_2 outline during horizontal loading. After (Larsen and Ibsen, 2006).

As it is intuitive the rotation of the line l_1 is equal to the angular coefficient a_1, which can be calculated with equation 5.3. Thereof the rotation is simply $\theta = \arctan(a_1)$. Once a_1 is known also a_2 can be calculated in virtue of the perpendicular lines property (equation 5.4).

$$a_1 = \frac{\Delta y_2 - \Delta y_1}{200} \tag{5.3}$$

$$a_2 = \frac{-1}{a_1} \tag{5.4}$$

Now, knowing the coordinates of the displaced points of measure, constants b_1 and b_2 can be calculated as:

$$b_1 = 95 + \Delta y_1 + a_1 \cdot 100 \tag{5.5}$$

$$b_2 = 120 - (\Delta x - 185) \cdot a_2 \tag{5.6}$$

Hereafter, the coordinates of the junction point s are calculated by using the equation $y_1 = y_2 = y_s$ which gives:

$$x_s = \frac{b_2 - b_1}{a_1 - a_2} \tag{5.7}$$

$$y_s = a_1 \cdot x_s + b_1 \tag{5.8}$$

Line l_1 midpoint is named m and by its determination the real displacement of the bucket foundation can be calculated.

$$x_m = x_s + 185 \cdot \cos(\theta) \tag{5.9}$$

$$y_m = y_s - 185 \cdot \cos(\theta) \tag{5.10}$$

Finally the horizontal displacement u and the vertical displacement w are obtained with the following relationships:

$$u = x_m - 95 \cdot \sin(\theta) \tag{5.11}$$

$$w = -(y_m - 95 \cdot \cos(\theta)) \tag{5.12}$$

In Figure 5.15 one displacement transducer on the right and one force transducer (or load cell) on the left are depicted. Before conducting the first of the six new tests the three LVDTs were calibrated by means of the calibration rig depicted in Figure 5.16.

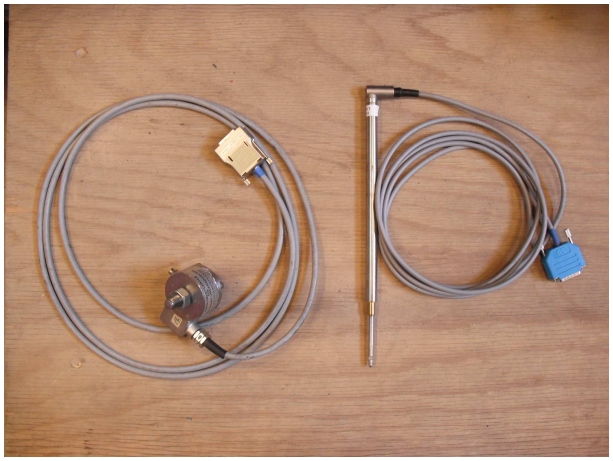

Figure 5.15: Force and displacement transducer.

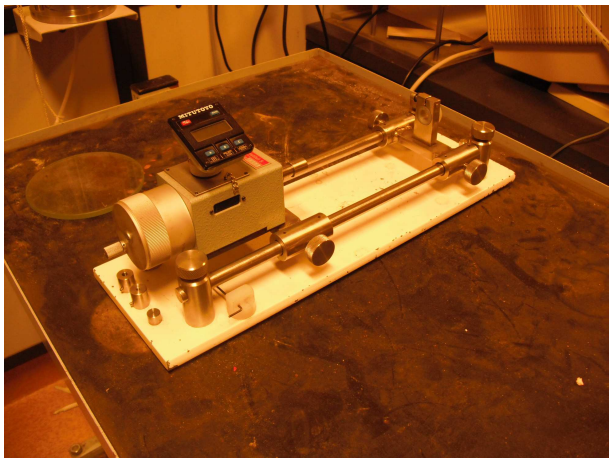

Figure 5.16: LVDTs calibration rig.

5.4 Forces Measurement

The moment at the soil surface was induced by a horizontal force H applied to a certain arm OH_3. Depending on the sort of load wanted, the horizontal load arm could be set. For the six new experiments the arm was set at 600 mm. Figure 5.17 represents the forces measurement system.

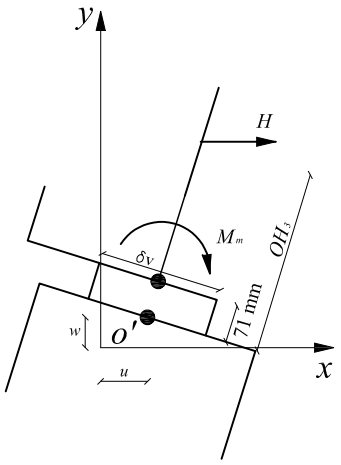

Figure 5.17: Forces and displacement on the bucket after Larsen and Ibsen (2006).

Two load cells, type HBM U2A 10 kN, were located 71 mm above the bucket lid, and measured the applied moment which is termed M_m. In actuality the cells measured the two vertical forces, and thereof, the moment was calculated as follow:

$$M_m = (V_1 - V_2) \cdot \delta V/2 \tag{5.13}$$

where V_1 and V_2 are the two vertical loads recorded by the load cells, whereas δV is the distance between the load cells. Thus, the corrected horizontal force is given

$$H_{corr} = \frac{M_m}{OH_3 - 71mm} \tag{5.14}$$

Hereafter the corrected moment M_0 can be calculated

$$M_0 = H_{corr} \cdot OH_3 \tag{5.15}$$

In case of suction applied, the two vertical load cells were not utilized because the playing forces exceeded the transducers capacity. In such cases

the moment was simply calculated as the measured horizontal force multiplied by the arm. To measure the horizontal load, one force transducer, type HBM U2A 100 kg, was mounted on the vertical bar, connected directly to the horizontal loading device. When the effective pressure was increased a load cell of the type HBM U2A 10 kN was utilized. Before commencing the first experiment all the transducers adopted have been calibrated by means of the force calibration rig shown in Figure 5.18.

Figure 5.18: Test Box, dimensions in mm.

All the presented devices are sketched in Figure 5.19.

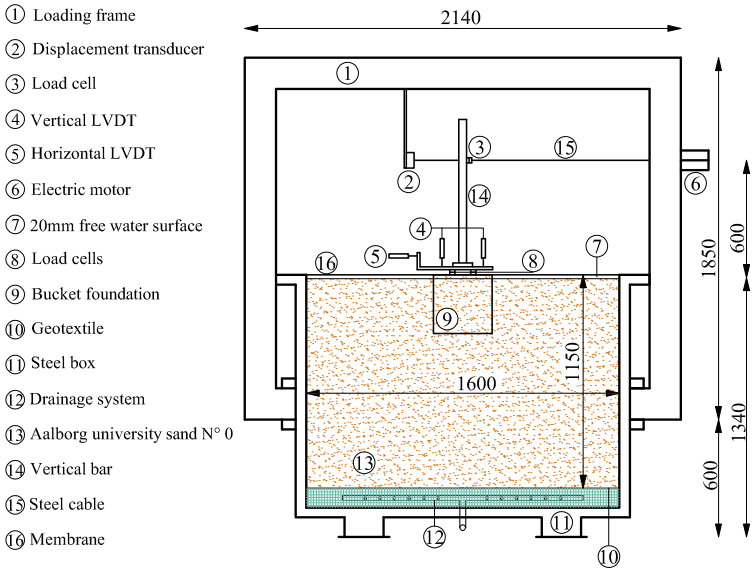

Figure 5.19: Test Box, dimensions in mm.

Chapter 6

Parameters of the Soil

In this chapter the sand used for conducting small-scale experiments on bucket foundations at the Geotechnical Laboratory at Aalborg University is introduced. Cone penetration test and relative calculation to estimate the soil parameters are presented in detail.

6.1 Aalborg University Sand No. 0

Aalborg University Sand No. 0 is a graded sand from Sweden. Small grains have sharp edges while large grain are rounded. Such sand is mostly composed by quartz. Also biotite and feldspar are contained. Its properties are shown in Table 6.1 (Ibsen, 1999).

Table 6.1: Index properties of Aalborg University sand No. 0. (Ibsen, 1999).

Property	Value	Unit
$d_{50} = 50\%$ - quantile	0.14	[mm]
$C_u = d_{60}/d_{10}$	1.78	[-]
Specific grain density d_s	2.64	[g/cm^3]
Maximum void ratio e_{max}	0.86	[-]
Minimum void ratio e_{min}	0.55	[-]

Ibsen and Bødker (1994) found by conducting sieve analysis the distribution of grains for Aalborg University sand No. 0 shown in Figure 6.1. Note that Aalborg University sand No. 0 is equal to Baskarp Sand No. 15.

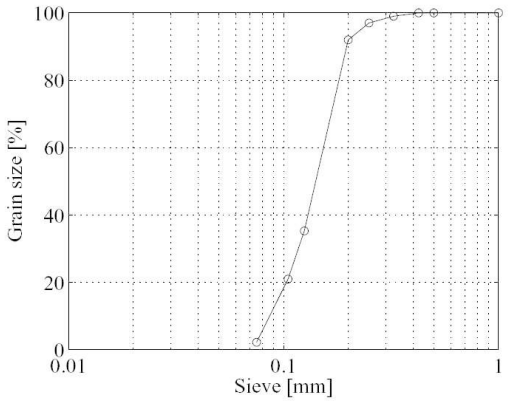

Figure 6.1: Distribution of grains for Aalborg University sand No. 0 from sieve analysis. (Ibsen and Bødker, 1994)

6.2 Cone Penetration Test

The homogeneity of the sand after the compaction procedure was tested by conducting a cone penetration test (CPT). In contrary to the traditional CPT used in situ, that utilized at Aalborg University laboratory measures only the tip resistance regardless of sleeves friction and pore pressure.

Figure 6.2: Cone Penetration Test device.

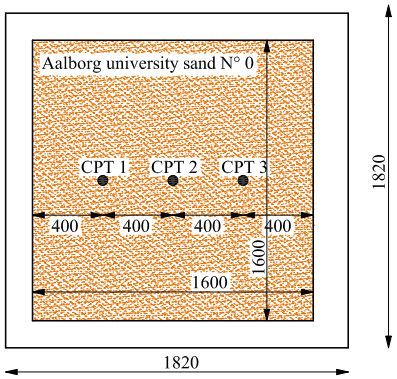

Figure 6.3: CPTs locations.

The tip resistance was measured by means of a full bridge strain gauge placed within the CPT body. To record the depth of the observations a displacement transducer was linked to the CPT device. A picture of the equipment used is illustrated in Figure 6.2. The CPT device was mounted on the loading frame and the test was conducted three times prior to each test. One CPT was conducted in the center of the tank and two CPTs were conducted 40 cm from the center on both sides, cf. Figure 6.3. The CPT penetration velocity was 5 mm/s and was kept steady at any depth. A typical result of the CPT series is illustrated in Figure 6.4. From Figure 6.4 it is seen that at three different locations the CPT gives very similar results, meaning an overall soil homogeneity. Figure 6.5 depicts the mean value of the CPTs conducted prior to each test. It can be noted that, fairly similar values are reached prior to each test.

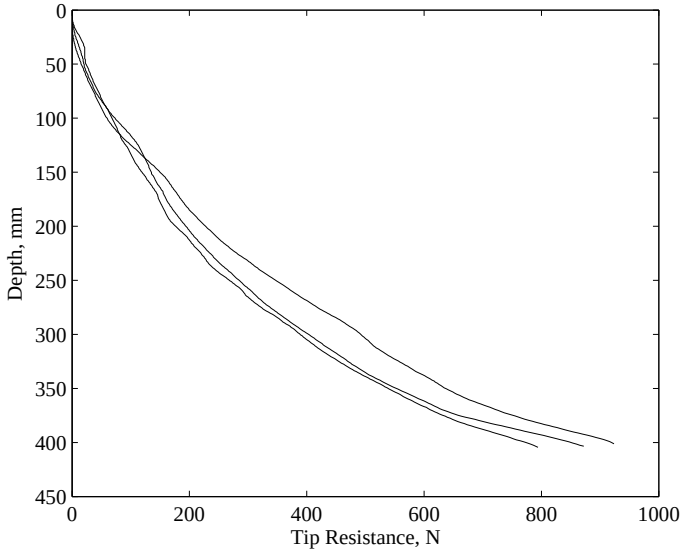

Figure 6.4: CPT result for test no. 2.

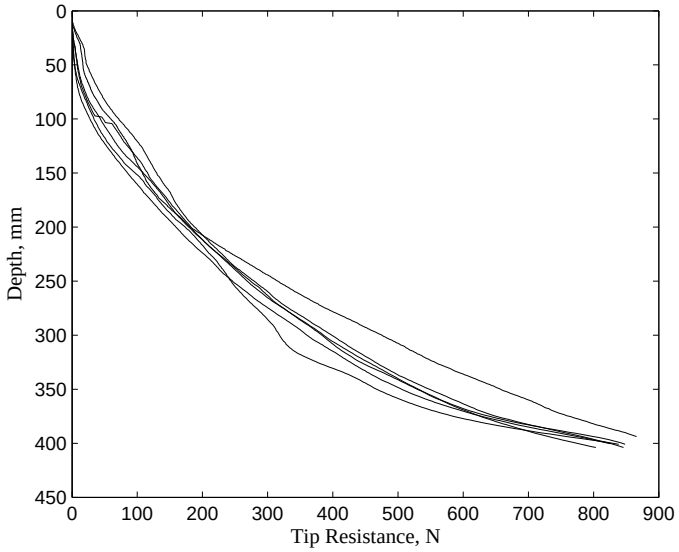

Figure 6.5: Comparison of CPTs result.

6.3 Soil Parameters Calculation

In order to obtain the density index, I_D, and thereof the other parameters of the soil from solely CPT data some calculations were made following Ibsen *et al.* (2009). The whole method was based on the relationship between density index and secant friction angle proposed by Schmertmann (1978). Such relationship was characterized for Aalborg University sand No. 0 by means of a series of triaxial tests.

Firstly an iteration process to find I_D was created following equations (6.1)-(6.4).

$$\gamma' = \frac{d_s - 1}{1 + e} \cdot \gamma_w \tag{6.1}$$

$$\sigma'_1 = \gamma' \cdot x \tag{6.2}$$

$$I_D = c_2 \cdot \left(\frac{\sigma'_1}{q_c^{c_1}} \right)^{c_3} \tag{6.3}$$

$$I_D = \frac{e_{max} - e}{e_{max} - e_{min}} \cdot 100 \tag{6.4}$$

Where σ'_1 is the effective vertical stress in MPa, e the effective void ratio, x the depth in m, γ_w the unit weight of the water in kN/m^3, q_c the cone resistance in MPa and, c_1, c_2, c_3 fitting constants corresponding to 0.75, 5.14, and -0.42 respectively. By employing equations (6.1)-(6.4) the void ratio e and the corresponding density index I_D were achieved at any depth after 4 to 5 loops. The requirement to fulfil the iteration was a difference between two successive e less than 10^{-4}. The process was initiated by setting $e = e_{min}$.

Thereafter also friction angle φ_{tr}, dilation angle ψ_{tr}, secant modulus of elasticity E_{50} and tangential modulus of elasticity E_0 were calculated by adopting equations (6.5)-(6.8). Note that the subscripts of the friction and dilation angle are "tr", as triaxial test results were mainly employed in determining

the below equations.

$$\varphi_{tr} = 0.152 \cdot I_D + 27.39 \cdot \sigma_3'^{-0.2807} + 23.21 \tag{6.5}$$

$$\psi_{tr} = 0.195 \cdot I_D + 14.86 \cdot \sigma_3'^{-0.09764} - 9.946 \tag{6.6}$$

$$E_{50} = (0.6322 \cdot I_D^{2.507} + 10920) \cdot \left(\frac{c \cdot cos\varphi_{tr} + \sigma_3' \cdot sin\varphi_{tr}}{c \cdot cos\varphi_{tr} + \sigma_3'^{ref} \cdot sin\varphi_{tr}} \right) \tag{6.7}$$

$$E_0 = \frac{2 \cdot E_{50}}{2 - R_f} \tag{6.8}$$

$$\tag{6.9}$$

where $\sigma_3'^{ref}$ is a reference pressure (100 kPa) while R_f is the failure ratio normally set to 0.9.

Note that equation (6.5) involves only φ_{tr} as unknown. Indeed σ_3' is plainly dependent on the coefficient of horizontal earth pressure at rest $K_0 = (1-\sin\varphi_{tr})$. Since the stress range inside the sand box in normal condition varies from 0 to 2.5 kPa, equation (6.5) converges only for enormously high φ_{tr} values. As a result of this, when the effective horizontal stress did not reach at least 5 kPa, the horizontal stress σ_3' of equation was set to 5 kPa. This assumption gives a friction angle slightly lower, but nevertheless acceptable. When the value of the effective stress exceeded 5 kPa, equation (6.5) could converge to reasonable value of φ_{tr}. Such case was that with 30 kPa of suction applied, at which horizontal stress was calculated as

$$\sigma_3' = \sigma_1' \cdot K_0 + P_0 \cdot K_0 \tag{6.10}$$

where P_0 is the increase of effective stress due to the suction. Material properties obtained from the CPTs conducted prior to the six tests are shown in Table **??**. The uncertainties related to the E_0 calculation were too high for most of the tests because of the very low stress state. Hence, the E_0 value was assessed only for test no. 4 which gave 19.8 Mpa. Tests in normal overburden pressure condition (tests no. 1 and 2) were conducted in saturated sand. The unit weight, γ, calculated was therefore the effective unit weight. When applying the increase in effective stress (tests no. 3, 4, 5 and 6)the soil was brought to dry condition. Hence, for those tests the dry unit weight of the soil was considered.

Table 6.2: Sand parameters for the six tests.

	φ_{tr} [°]	ψ_{tr} [°]	I_D [-]	γ [kN/m^3]
Test 1	52.31	17.72	0.77	10.61
Test 2	52.28	17.67	0.76	10.59
Test 3	51.92	17.21	0.74	15.88
Test 4	51.87	16.13	0.72	15.82
Test 5	51.63	16.85	0.72	15.82
Test 6	51.25	16.37	0.70	15.76

The above approach was used only for the six novel tests. The reader should refer to Larsen (2008) for information about soil parameters calculation employed in previous bucket foundations experiments.

Chapter 7

Small-Scale Testing of Laterally Loaded Bucket Foundations in Dense Sand

Monopod bucket foundations promise to become a reliable and cost-effective option for offshore wind turbine foundations. In this chapter, six small-scale tests of a steel bucket foundation subjected to quasi-static lateral load, are presented. When conducting small-scale experiments on soil, scale effects can considerably affect the tests outcome. To overcome this issue, a novel testing system based on the application of a suction between the soil surface and a membrane, is employed. By means of the suction the effective stress of the soil is increased. The tests are conducted at stress levels of 0 kPa, 10 kPa, 15 kPa, 20 kPa, and 30 kPa ,respectively. The test results successfully prove reliability and consistency of the method. The comparison between the tests conducted at stress level of 0 kPa, and the tests with stress level increased, shows remarkable differences. The rotation reached at soil failure is higher for tests performed with increased effective stress. The relationship between scaled overturning moment, $M/(\gamma \cdot d^4)$, and rotation, is well represented by a power law. The exponent of the power law is consistent among all tests carried out with stress level increased. Besides, attention is given to the instantaneous centre of rotation paths during loading, unloading and reloading phases. Further cyclic loading studies may adopt this testing system to better investigate the accumulated rotation of bucket and monopile foundations.

7.1 Testing Programme

The test program consisted of 6 monotonic horizontal loading tests of the bucket foundation at five different effective stress level. All experiments took place at the Geotechnical Engineering Laboratory at Aalborg University. According to the scaling relationship proposed in Chapter 4, the tests features were chosen in order to model the behaviour of a real bucket foundation with

$d = 16$ m, $D = 16$ m, $h = 32$ m. The arm of the horizontal load , h, refers to the waves action. The foundation adopted to carry out all tests was a steel bucket of diameter, $D = 300$, with a skirt of $d = 300$, cf. Figure 7.1. The arm of the horizontal force h was for every test 600 mm from the soil surface.

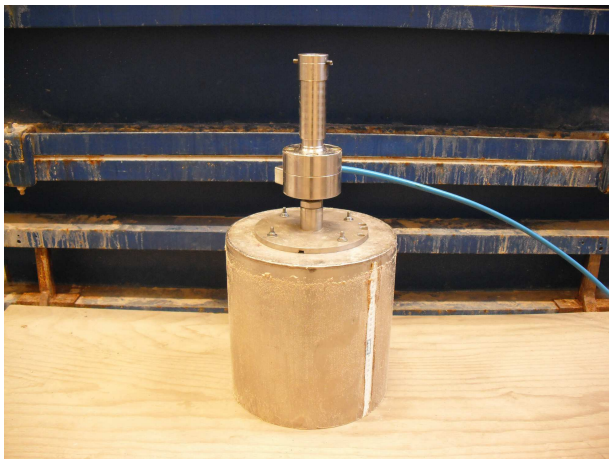

Figure 7.1: 300 mm diameter, 300 mm skirt bucket foundation.

Tests were performed at different soil effective pressure. The test program is listed in Table 7.1.

Table 7.1: Test program.

Test No.	Overburden Pressure [kPa]
1	0
2	0
3	15
4	30
5	20
6	10

7.2 Results

Part of the following results will be presented employing the dimensionless moment $M/(\gamma \cdot d^4)$ and the dimensionless horizontal force $H/(\gamma \cdot d^3)$. The choice of these normalized values relies on the results found in Chapter 4 regarding the dimensionless relationships moment-rotation, and horizontal load-displacement. Hereby, attention is mainly given to the relationship between dimensionless moment and rotation, which is more relevant for bucket foundation fatigue design.

Test no. 1 and test no. 2 were performed to have a double check of the case without overburden pressure increased. Indeed, they give basically the same response in terms of loading as well as in terms of deformation. Although test no. 3 was too early interrupted, its result is considered significant and it is not dismissed from the data analysis.

7.2.1 Force-Displacement Curves

The raw moment data for all tests, as collected with rotation, are presented in Figure 7.2. In the figure legend, the suction at which each test was carried out, is stated. In every test the soil was brought to failure. As it was expected, when the effective stress is increased the failure occurs at higher value of both applied moment and rotation. From Figure 7.2, it can be observed that the moment-rotation gradient diminishes significantly after 2° of rotation for test no. 3, 4, 5, and 6, and after 1° of rotation for Test no. 1. Starting from 1.5 °, in tests no. 3, 4, and 5, a series of sudden load-loss immediately followed by a load-recover, can be noted. This attribute may be due to the dilation of the sand which involves more and more soil during the development of the failure mode. Indeed when this phase ceases the load increases at a lower rate than before. Such phenomena does not occur when the overburden pressure is not increased and when the suction is 10 kPa. Figure 7.2 illustrates also how, the applied moment, strongly depends on the overburden pressure. For instance, the bucket foundation rotation equal to 1° is obtained with a moment of approximately 130 Nm for test no. 1 and 2. With respect to the latter value, the moment increases with a factor of approximately 6.4, 8.2, 9.7, and 12.7 for test no. 6, 3, 5, and 4 respectively. Similar observation can be made for the horizontal load-horizontal displacement curves shown in Figure 7.3. The residual plastic deformation seems to be independent of the overburden pressure state. After the unloading phase the plastic deformation falls within the range 80-90 %

of the deformation reached after the loading phase. Experiments conducted by **?** with normal overburden pressure conditions, revealed the same residual plastic deformation.

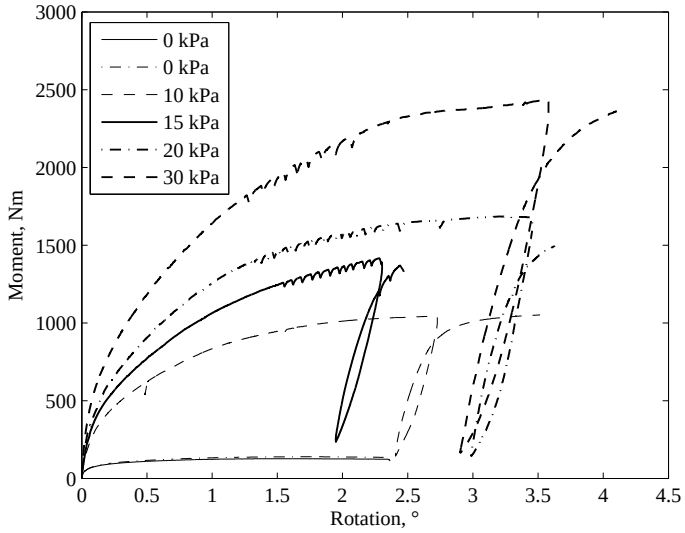

Figure 7.2: Raw rotation-moment data for all tests.

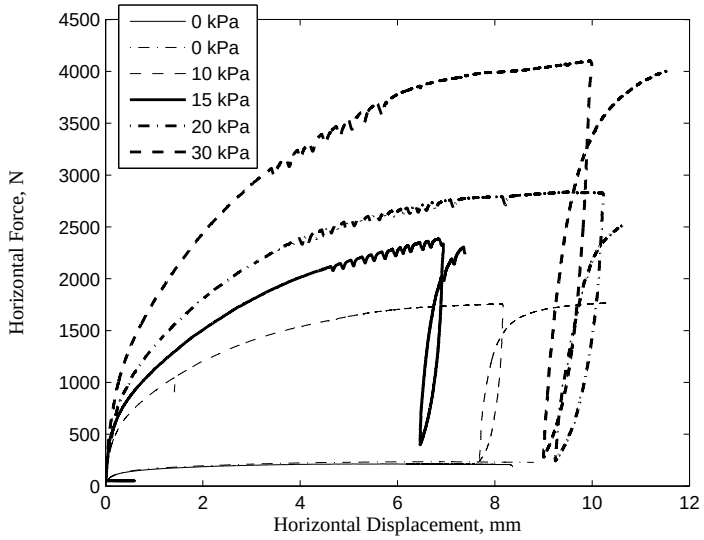

Figure 7.3: Raw data of horizontal displacement-horizontal force, for all tests.

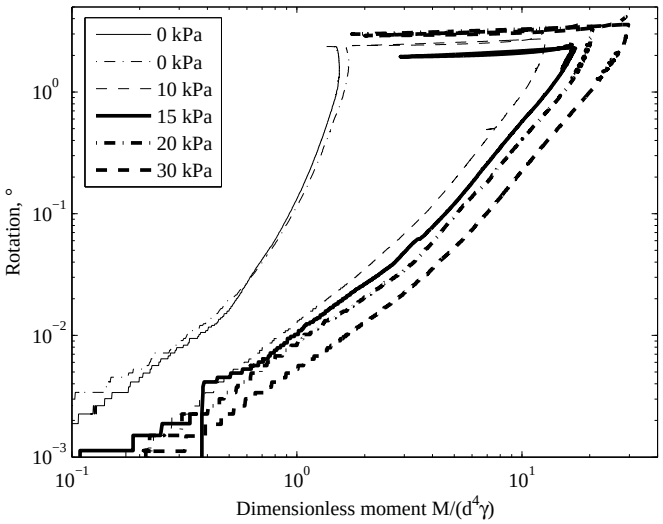

Figure 7.4: Raw dimensionless moment-rotation data for all the tests on a logarithmic plane.

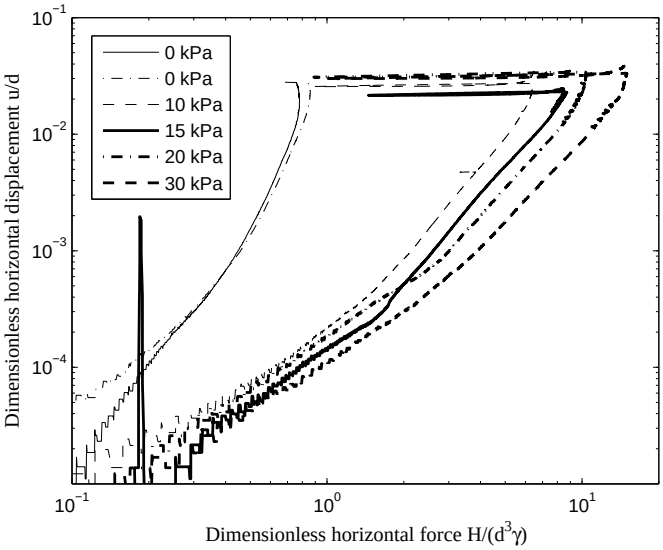

Figure 7.5: Raw dimensionless moment-rotation data for all the tests on a logarithmic plane.

In Figure 7.4 raw data of the bucket foundation rotation against the dimensionless overturning moment, $M/(\gamma \cdot d^4)$, are plotted on double logarithmic scale. The same plot concerning normalized horizontal force-horizontal displacement is given in Figure 7.5. In both figures, the records of tests with

increased effective stress show a distinct similar slope which contrasts with that of test no. 1 and 2. Focusing now on the first 0.5° of rotation, *i.e.* significant for fatigue limit states, a power law by the analytical form

$$\theta = \left(\frac{M}{\gamma \cdot d^4}\right)^{\mu} \cdot C \tag{7.1}$$

can be adopted to represent the records (see Chapter 4). In Figure 7.6 the rotation as a function of the dimensionless moment is given only for the first 0.5 ° of rotation. In order to avoid data superposition test no. 2 is not displayed in Figure 7.6. Although the power law shows slightly lower values of $M/(\gamma \cdot d^4)$ for rotation $\theta < 0.05°$, it is considered well representative of the normalized moment-rotation trends.

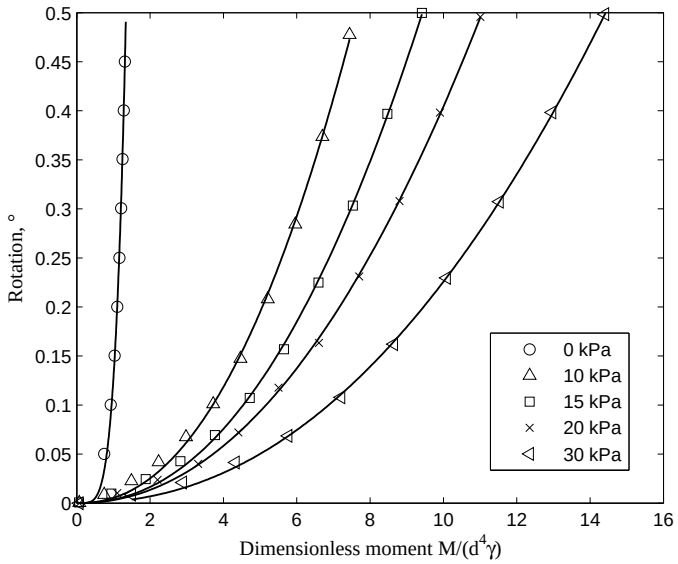

Figure 7.6: Dimensionless moment-rotation curves, each of them fitted with a power law.

In Table 7.2 a Comparison of the power law analytical expressions is given. The exponent of the tests with suction applied is consistent and differs from the exponent of tests no. 1 and no. 2. This suggests that when the soil effective stress is increased the value of exponent μ is constant.

Table 7.2: Power law coefficients for every test.

	Suction [kPa]	C [-]	μ [-]
Test 1	0	0.127	4.64
Test 2	0	0.11737	3.98
Test 6	10	0.01425	2.23
Test 3	15	0.00965	2.20
Test 4	20	0.00791	2.11
Test 5	30	0.00402	2.17

The ultimate moment capacity of the bucket foundation, under different overburden pressure induced, is taken as the moment measured at 3° of rotation. For test no. 3 a spline interpolating function is adopted to obtain the moment at 3° of bucket rotation, cf. Figure 7.7. Although test no. 1 and test no. 2 do not reach 3° of rotation, the moment ceases to increase after 1° of rotation. Therefore, the ultimate moment capacity of these tests was taken as the maximum moment reached during the tests. Table 7.3 lists the ultimate moment for all tests.

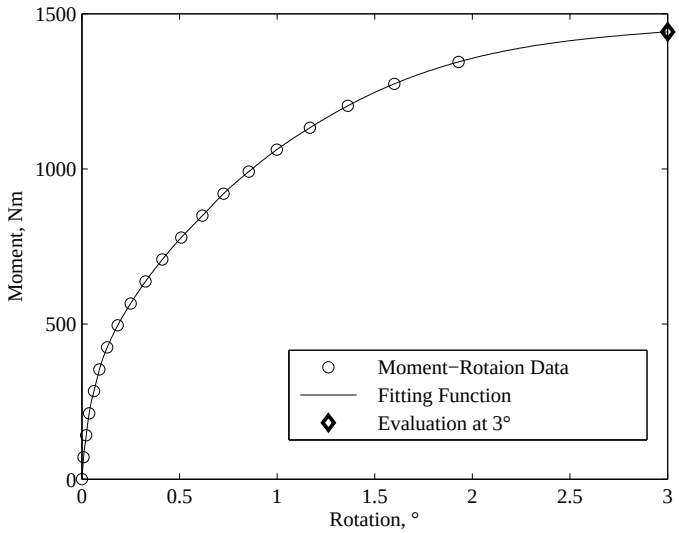

Figure 7.7: Evaluation of the ultimate moment for test no. 3.

Table 7.3: Ultimate moment capacity.

Test no.	Ultimate Moment Capacity [Nm]
1	213
2	234
6	1008
3	1444
4	1674
5	2401

7.2.2 Displacements Analysis

In Figure 7.8 the horizontal displacement, u, is plotted as a function of the rotation, θ, for each test. Every record exhibits a linear trend. A gap between tests conducted in normal stress conditions, and those at increased effective stress, is evident. This indicates that, the failure mode of the two cases is, to some extend, different. This is plausible, and can be attributed to the different stress states distribution in case of overburden pressure increased. By computing the LVDTs measurements the instantaneous centre of rotation could be evaluated. In Figure 7.9 the istantaneous centre of rotation for test no. 1 are illustrated. A typical instantaneous centres of rotation distribution for tests with effective stress increased is illustrated in Figure 7.10, where only the loading phase path of test no. 5 is considered. In both figures, the arrow above the graph, indicates the loading direction. The majority of the instantaneous centres of rotation was found below the middle of the skirt, toward the direction of the loading. In spite this general similarity, a little difference between the two plots can be noted. The centres of rotation for test no. 1 are concentrated lower, and more toward the loading direction.

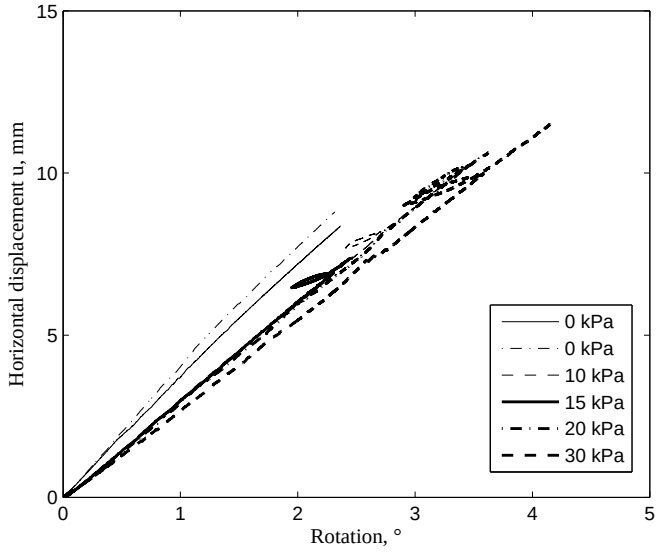

Figure 7.8: Horizontal displacement against rotation.

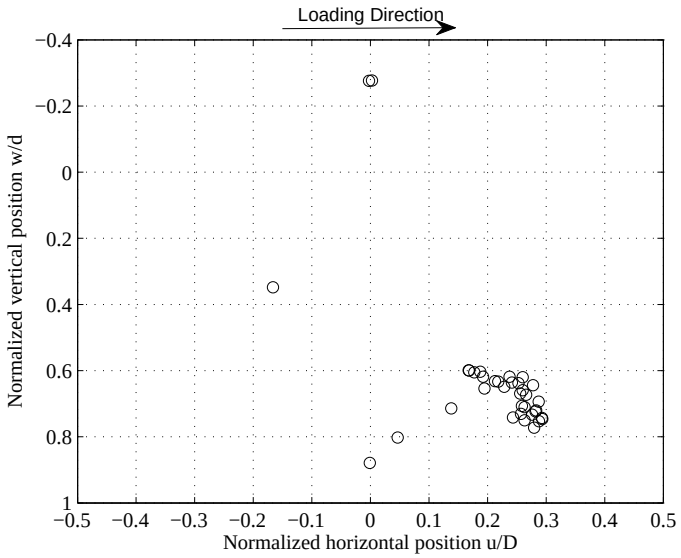

Figure 7.9: Instantaneous centres of rotation for test no. 1.

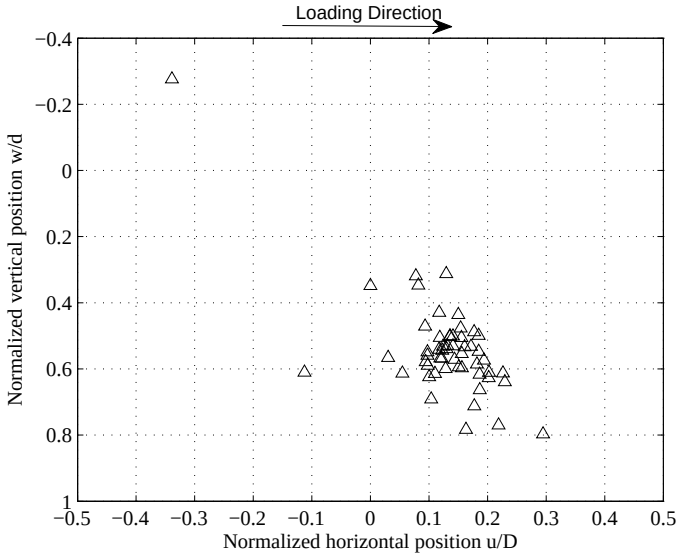

Figure 7.10: Instantaneous centres of rotation for test no. 5.

7.3 Conclusions

Bucket foundations may become a cost-effective option for offshore wind turbine support. Over the last decade small-scale experiments and field trials have proven the reliability of these foundations. The loads acting on an offshore structure are mainly cyclic and the current aim of researchers is addressing the cyclic loading response of such structures.

In a bid to minimize the scale effect of further cycling loading small-scale tests a new testing method is set out in this paper. The novel method consists of applying a suction between a membrane and the soil surface in order to increase the soil effective stress.

The results clearly shown how the moment applied on the bucket depends on the stress state of the soil. The consistency of the method was achieved by proving that, stiffer responses of the soil correspond to higher overburden applied by means of the suction. The plastic response of the soil was not affected by the different overburden pressure applied. The normalized moment-rotation curves of tests with increased overburden pressure followed a peculiar tendency. The overturning moment capacity was calculated for every test. This will be useful to calibrate the load magnitude of cyclic loading tests. Due to the distinct boundary conditions, tests in normal conditions showed a slightly different failure mode than tests with overburden pressure increased. This conclusion was reached by plotting rotation against horizontal displacement curves and by analysing the instantaneous centres of rotation locations of different tests. Further numerical simulations have to take heed of the different failure mode presented by the tests with effective stress increased.

The overall method was found to be consistent and gave the expected results. Interesting information for future cyclic loading researches were obtained.

Appendix A

Tests Data

Throughout this appendix the data obtained by conducting six quasi-static tests of a bucket foundation are presented. For each test, also the graphs regarding CPTs performed to verify the homogeneity of the sand are shown. In the figure caption of some figures, eventual notes on the test are pointed out.

Figure A.1: Overview of the experiments rig.

A.1 Test no. 1, no suction applied

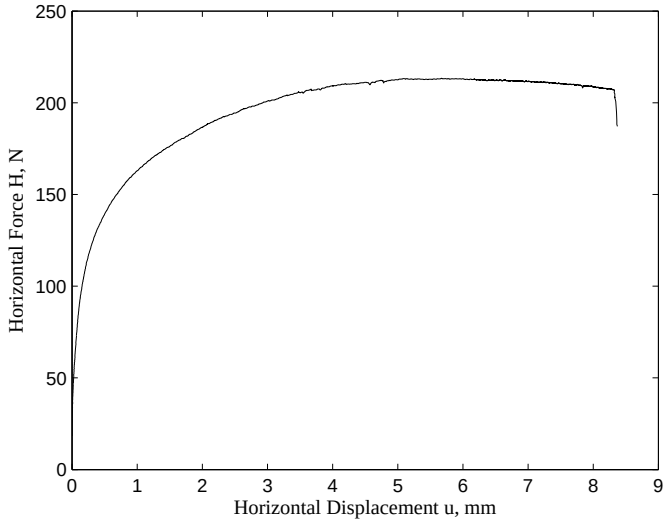

Figure A.2: Horizontal force-horizontal displacement, Test 1.

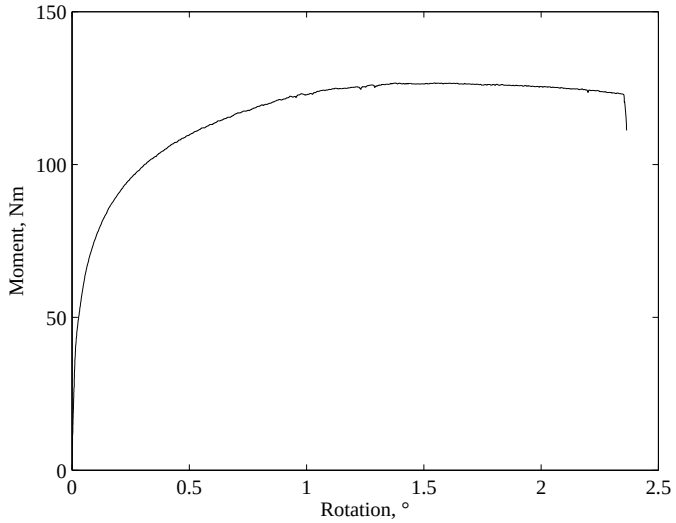

Figure A.3: Moment-Rotation, Test 1.

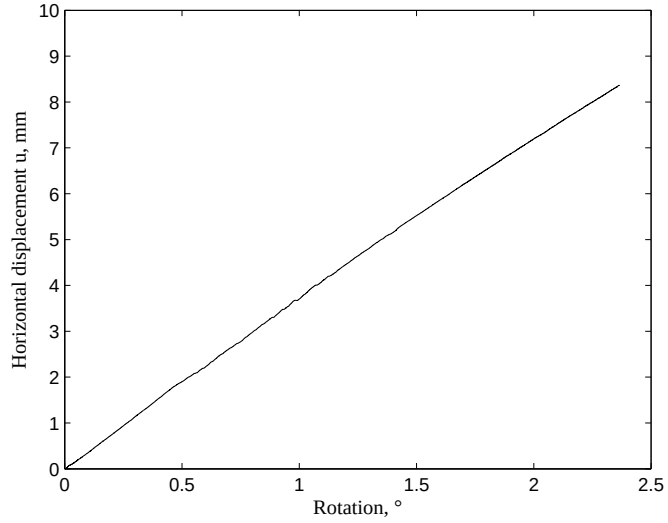

Figure A.4: Displacement against rotation.

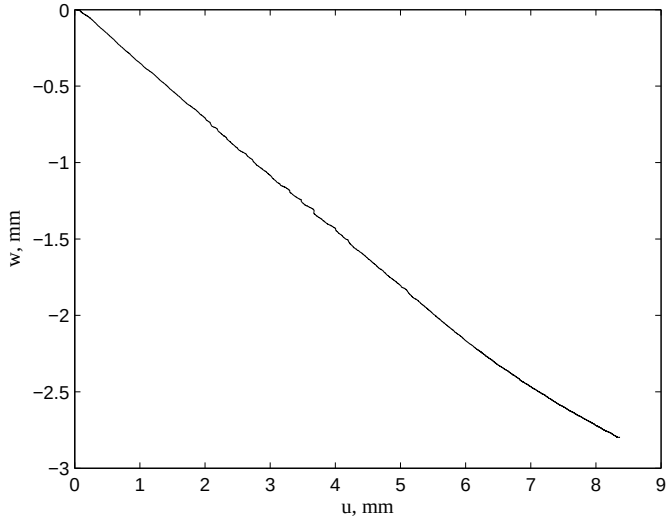

Figure A.5: Displacement of the bucket during Test 1.

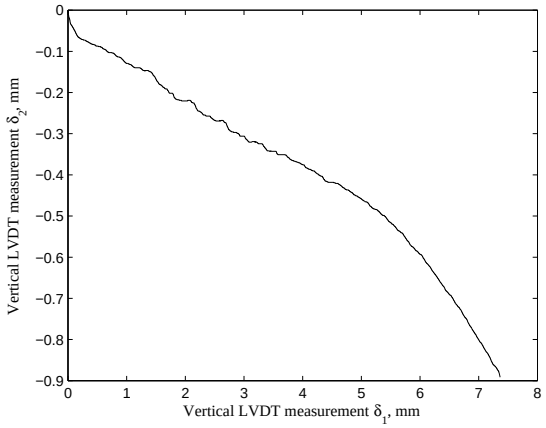

Figure A.6: LVDTs measurements during Test 1.

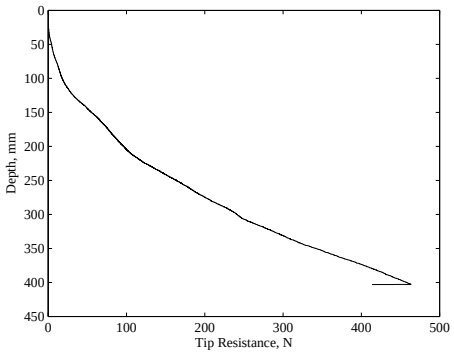

Figure A.7: Test1, CPT 1, the calibration was likely wrong when conducting this CPT.

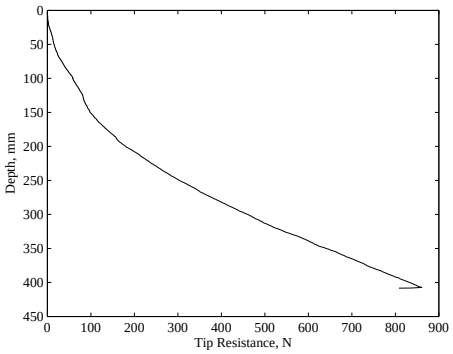

Figure A.9: Test1, CPT 3.

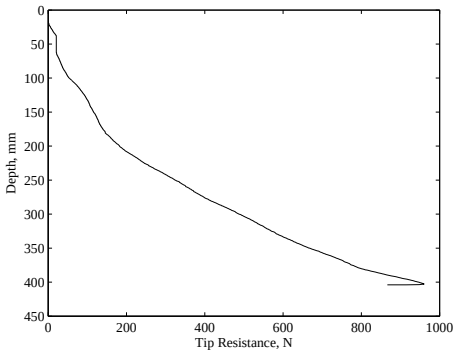

Figure A.8: Test1, CPT 2.

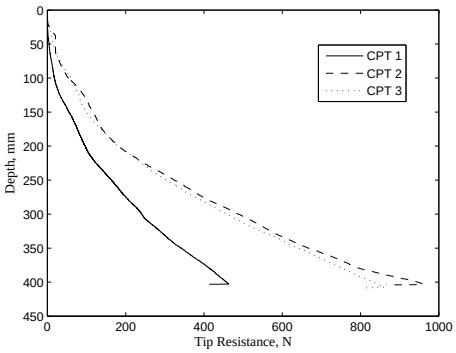

Figure A.10: Comparison of CPTs.

A.2 Test no. 2, no suction applied

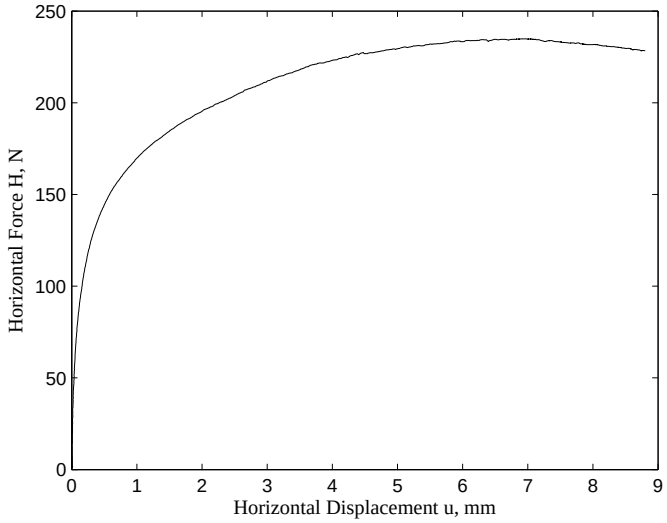

Figure A.11: Horizontal force-horizontal displacement, Test 2.

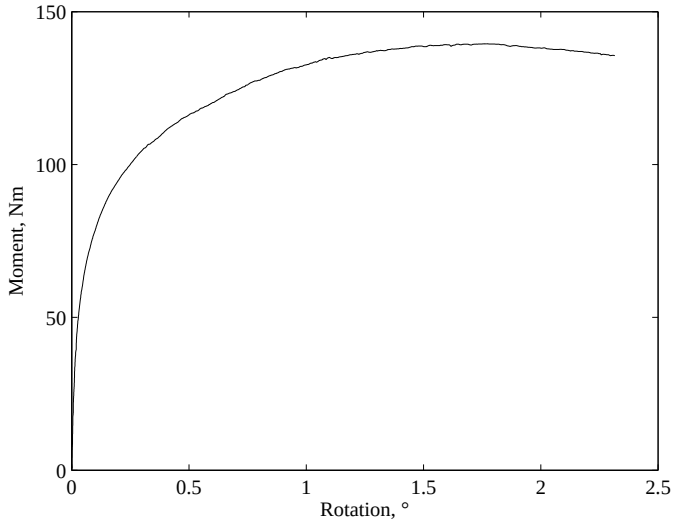

Figure A.12: Moment-Rotation, Test 2.

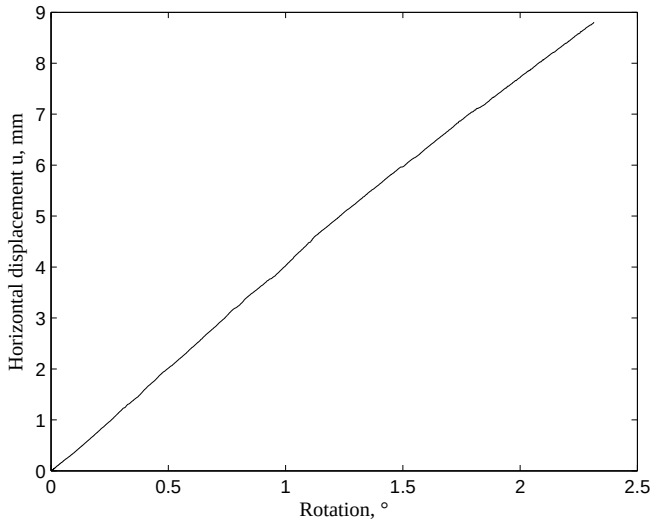

Figure A.13: Displacement against rotation.

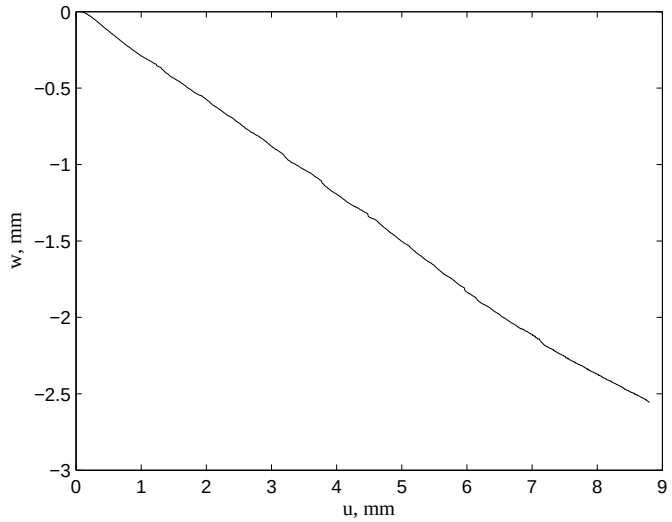

Figure A.14: Displacement of the bucket during Test 2.

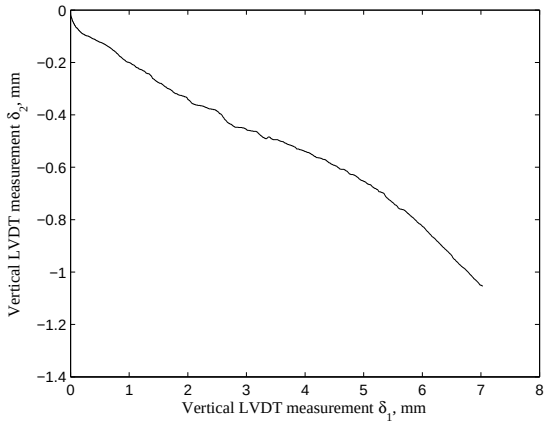

Figure A.15: LVDTs measurements during Test 2.

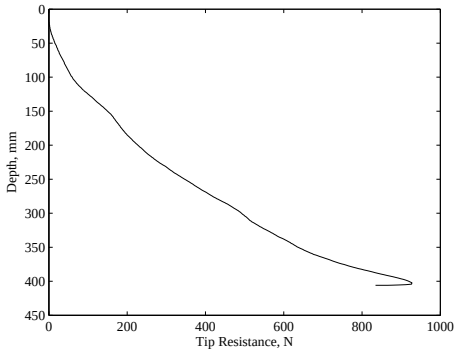

Figure A.16: Test2, CPT 1.

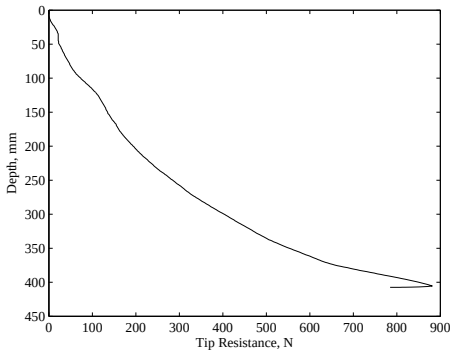

Figure A.17: Test2, CPT 2.

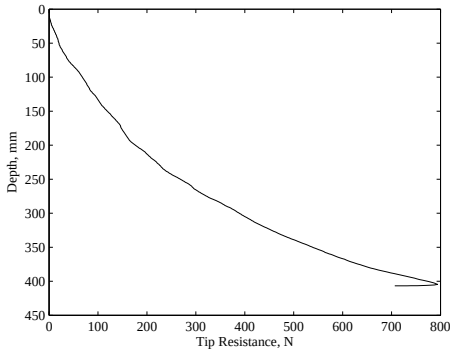

Figure A.18: Test2, CPT 3.

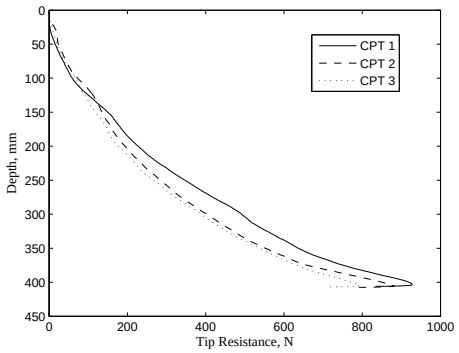

Figure A.19: Comparison of CPTs.

A.3 Test no. 3, 15 kPa suction applied

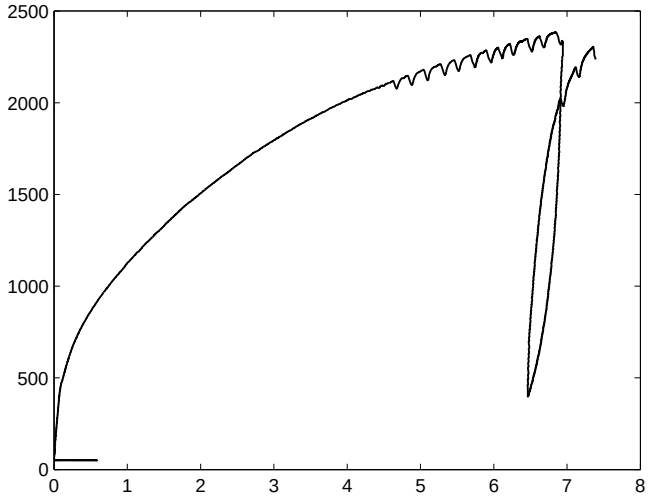

Figure A.20: Horizontal force-horizontal displacement, Test 3.

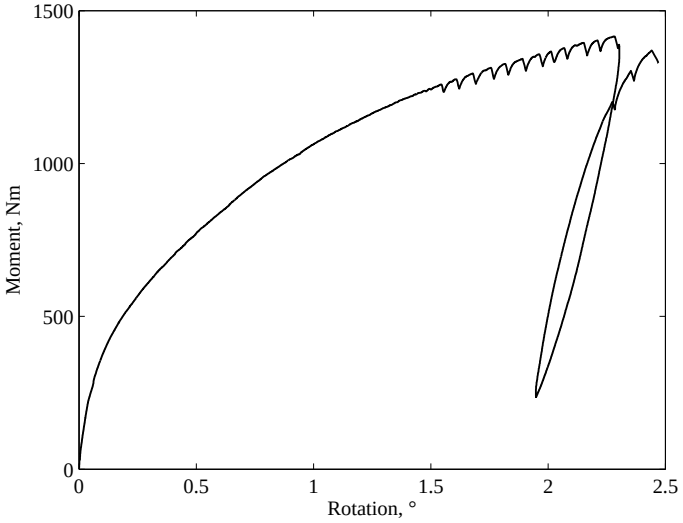

Figure A.21: Moment-Rotation, Test 3.

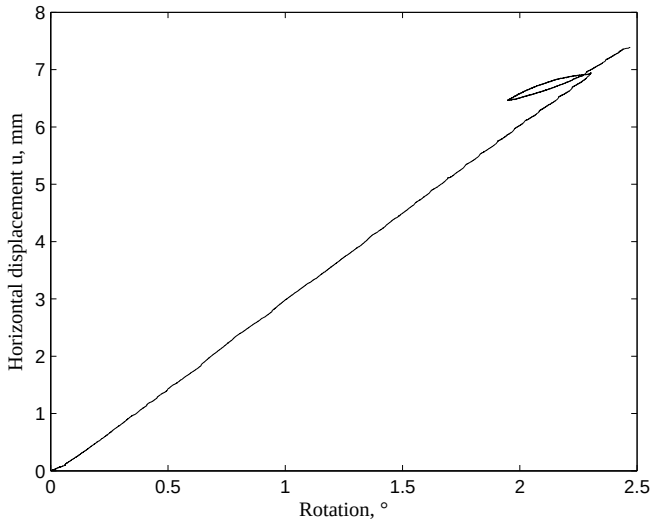

Figure A.22: Displacement against rotation.

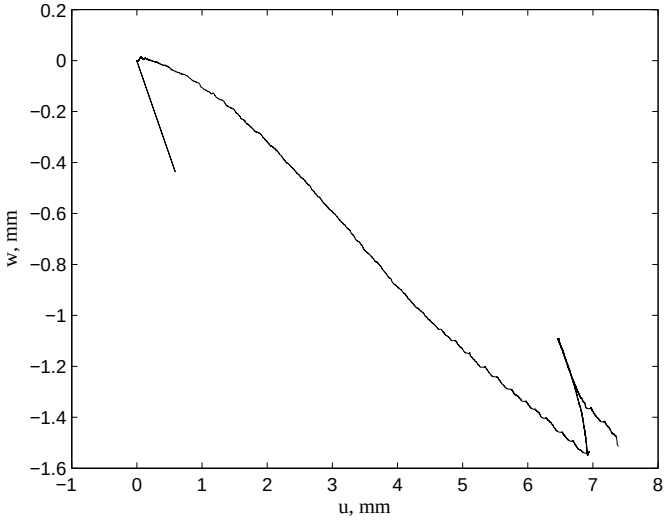

Figure A.23: Displacement of the bucket during Test 3.

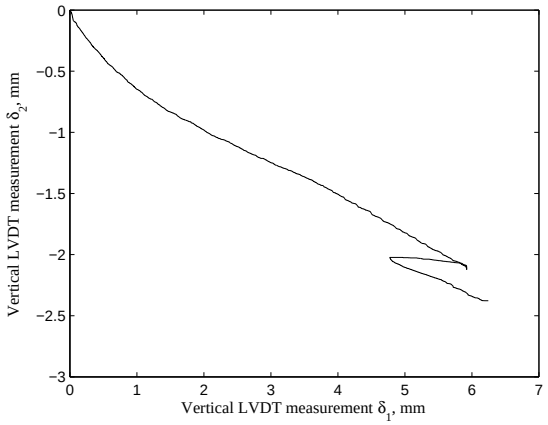

Figure A.24: LVDTs measurements during Test 3.

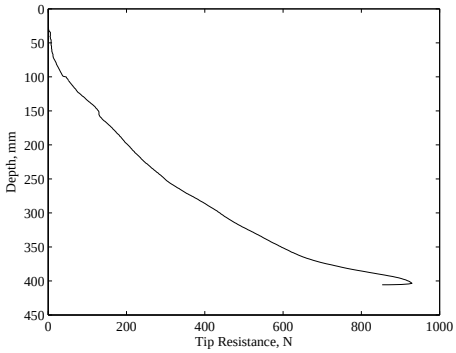

Figure A.25: Test3, CPT 1.

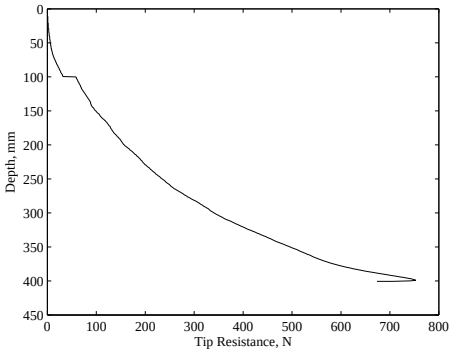

Figure A.27: Test3, CPT 3.

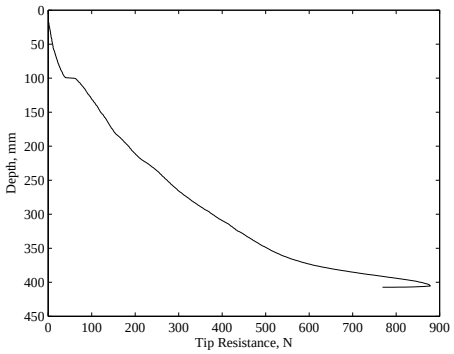

Figure A.26: Test3, CPT 2.

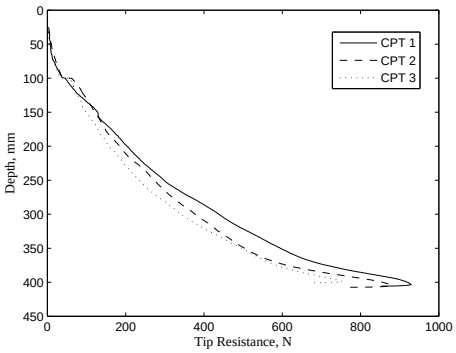

Figure A.28: Comparison of CPTs.

A.4 Test no. 4, 30 kPa suction applied

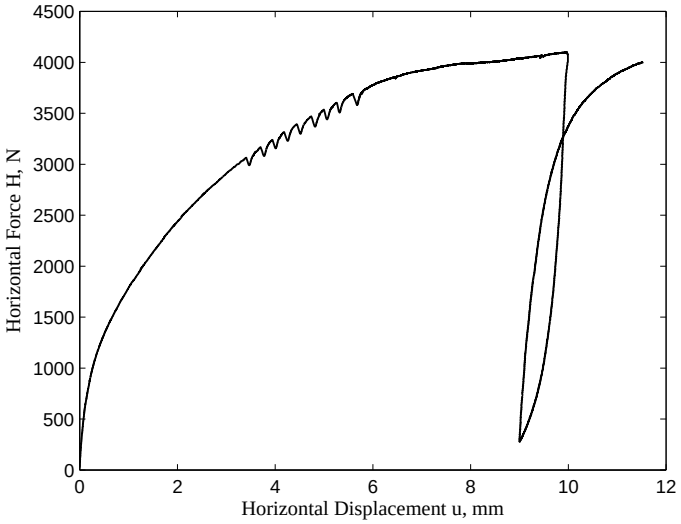

Figure A.29: Horizontal force-horizontal displacement, Test 4.

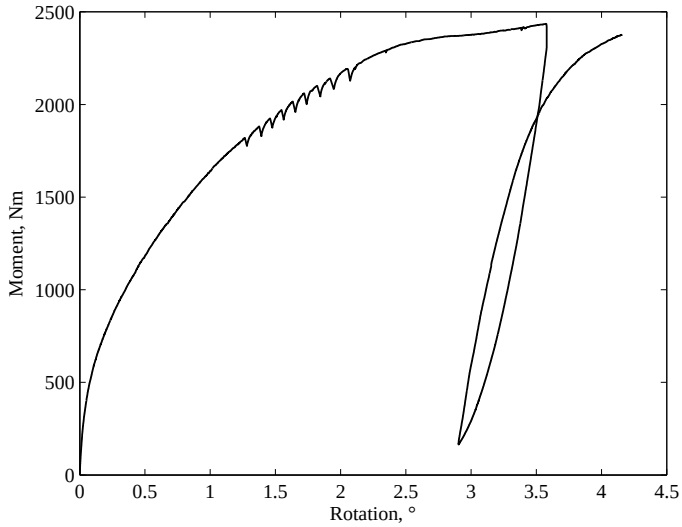

Figure A.30: Moment-Rotation, Test 4.

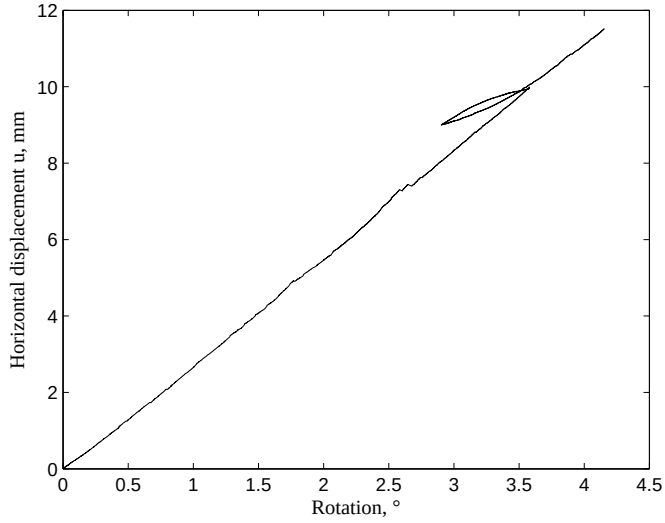

Figure A.31: Displacement against rotation.

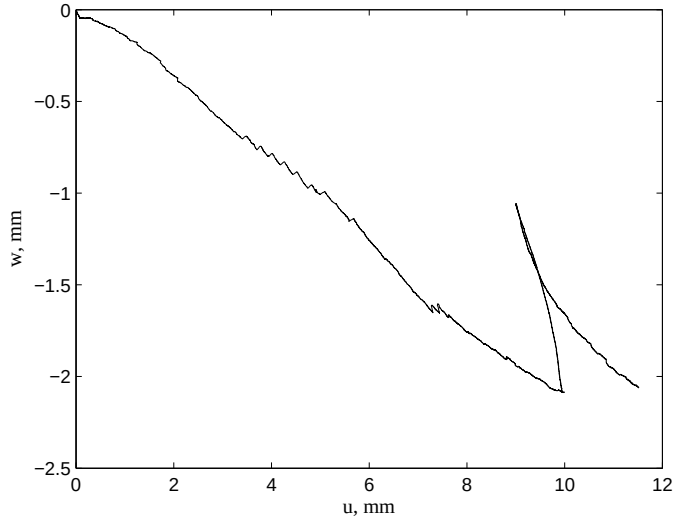

Figure A.32: Displacement of the bucket during Test 4.

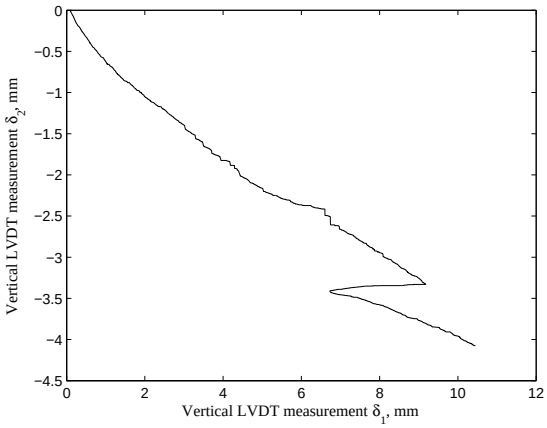

Figure A.33: LVDTs measurements during Test 4.

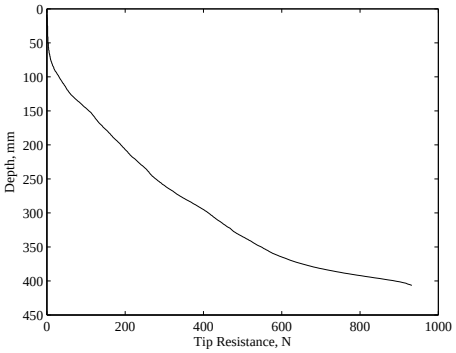

Figure A.34: Test4, CPT 1.

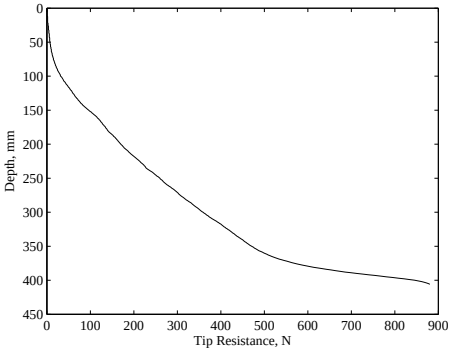

Figure A.35: Test4, CPT 2.

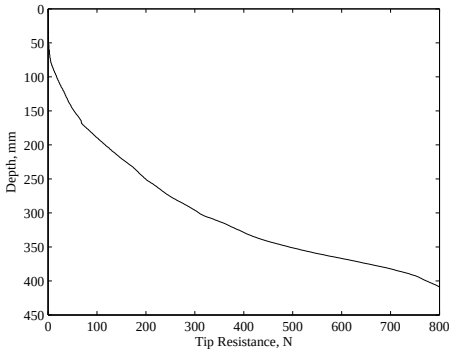

Figure A.36: Test4, CPT 3.

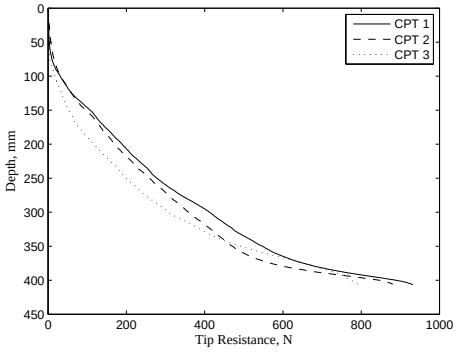

Figure A.37: Comparison of CPTs.

A.5 Test no. 5, 20 kPa suction applied

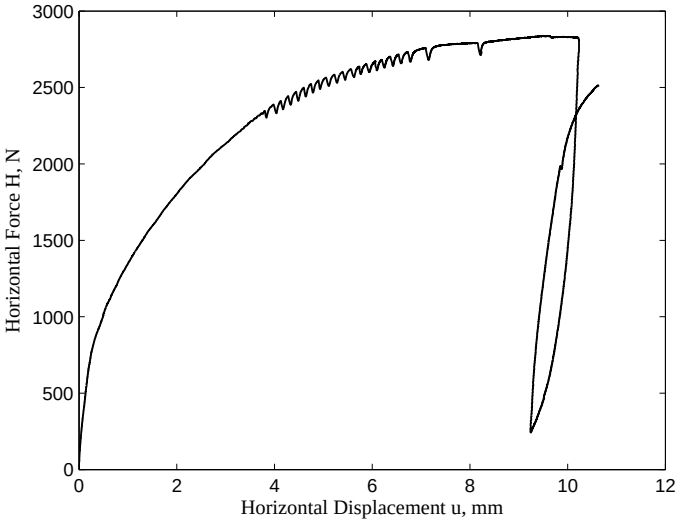

Figure A.38: Horizontal force-horizontal displacement, Test 5.

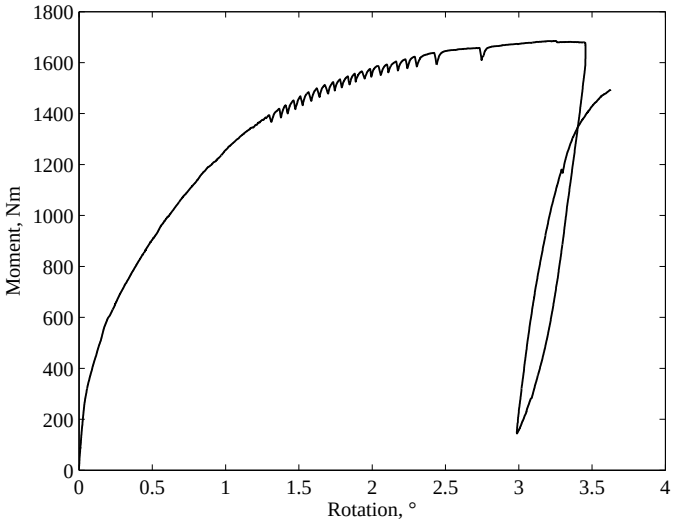

Figure A.39: Moment-Rotation, Test 5.

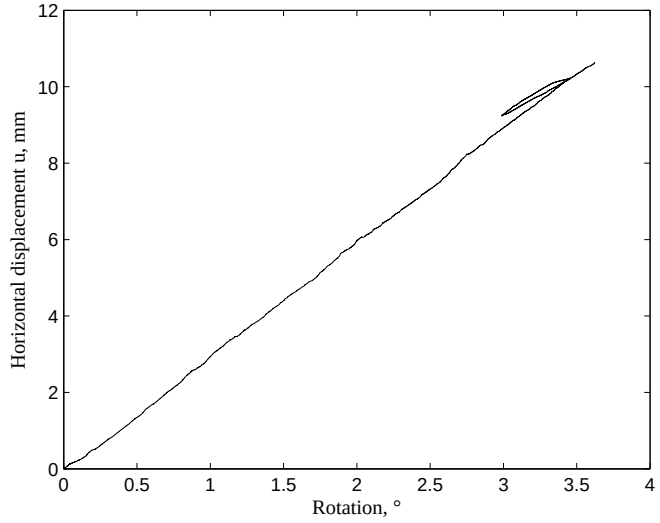

Figure A.40: Displacement against rotation.

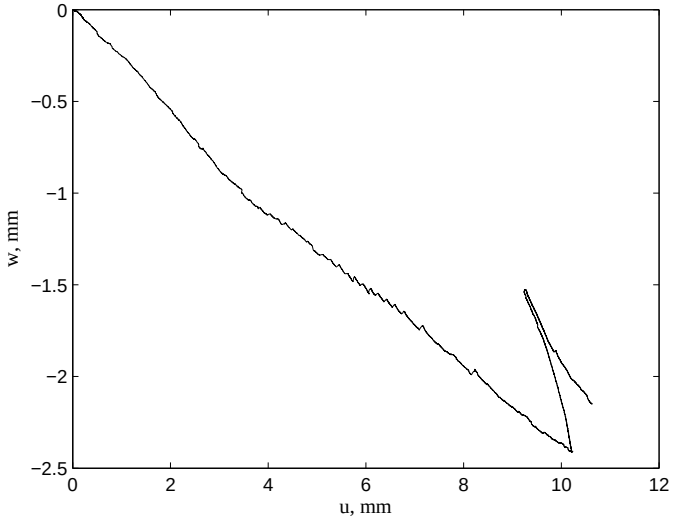

Figure A.41: Displacement of the bucket during Test 5.

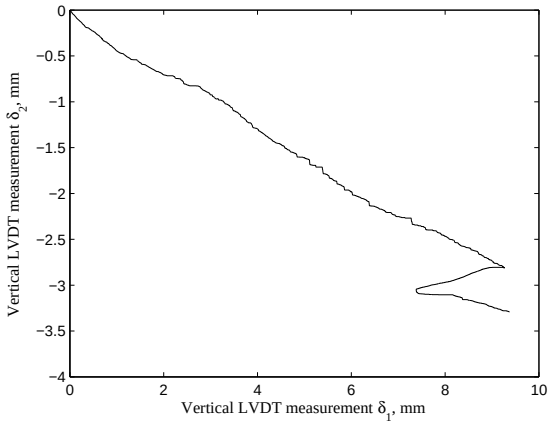

Figure A.42: LVDTs measurements during Test 5.

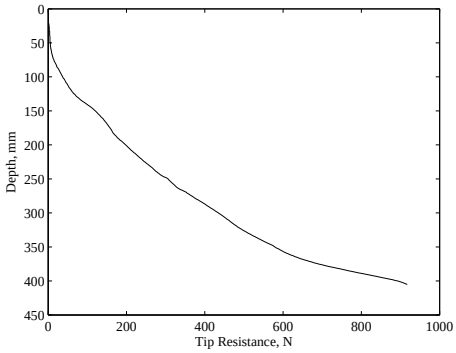

Figure A.43: Test5, CPT 1.

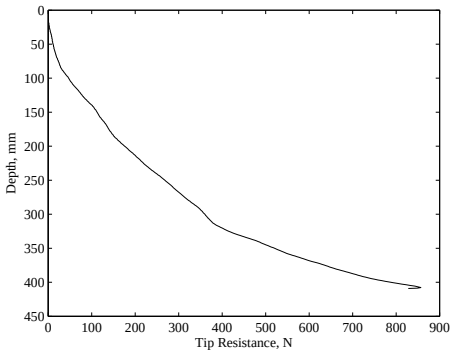

Figure A.44: Test5, CPT 2.

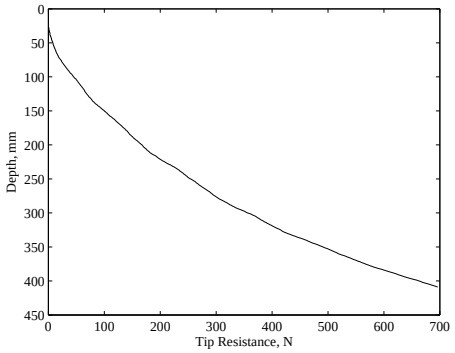

Figure A.45: Test5, CPT 3.

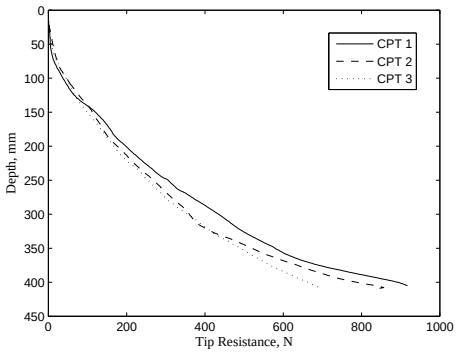

Figure A.46: Comparison of CPTs.

A.6 Test no. 6, 10 kPa suction applied

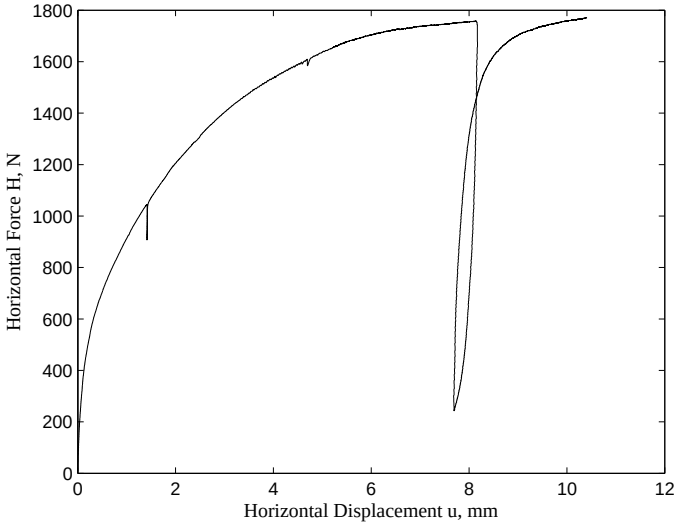

Figure A.47: Horizontal force-horizontal displacement, Test 6.

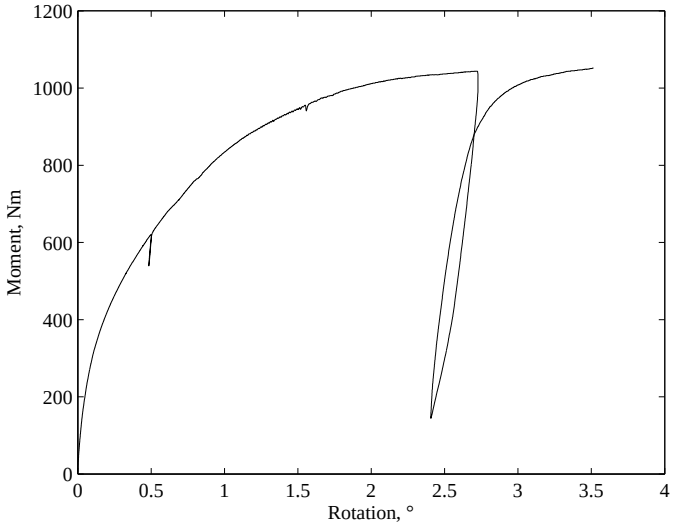

Figure A.48: Moment-Rotation, Test 6.

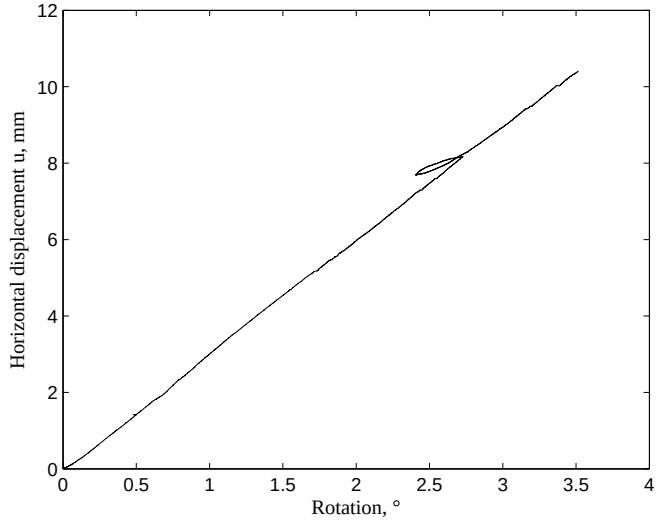

Figure A.49: Displacement against rotation.

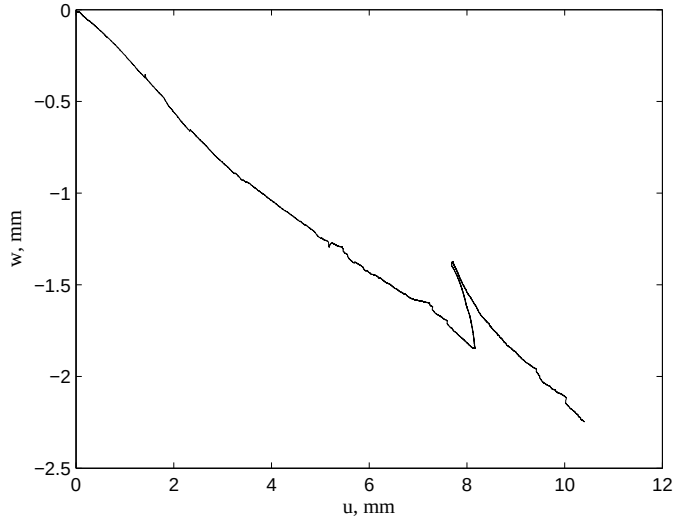

Figure A.50: Displacement of the bucket during Test 6.

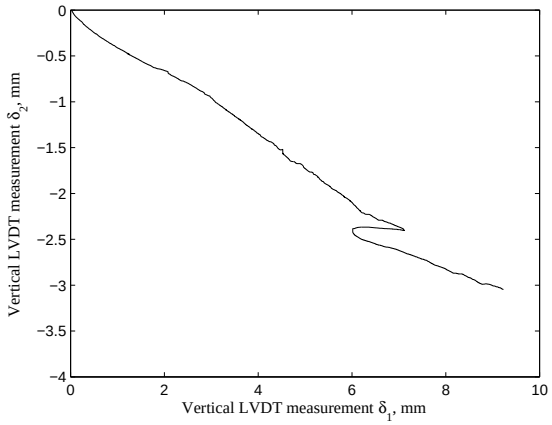

Figure A.51: LVDTs measurements during Test 6.

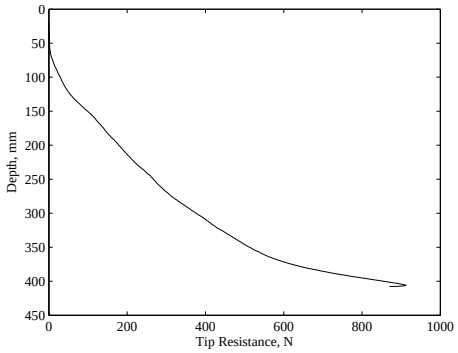

Figure A.52: Test6, CPT 1.

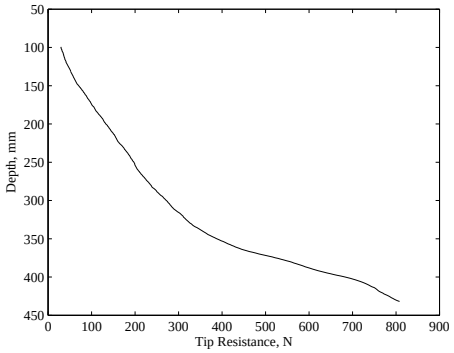

Figure A.54: Test6, CPT 3.

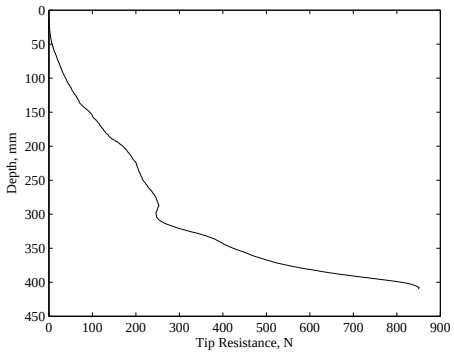

Figure A.53: Test6, CPT 2.

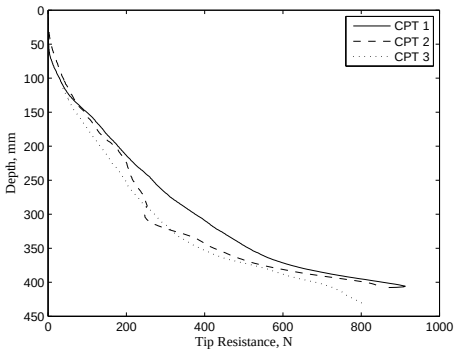

Figure A.55: Comparison of CPTs.

Bibliography

Achmus, M., Yu-Shu Kuo, Khalid Abdel-Rahman (2008). Behavior of monopile foundations under cyclic lateral load, *Computer and Geotechnics* 36, 725-735.

Achmus, M., Albiker, J., Abdel-Rahman, K. (2010). Investigation on the behaviour of large diameter piles under cyclic lateral loading, *Proceedings of the international symposium on Frontiers in offshore geotechnics II*, Perth Australia, November 2010.

API (2002). *Recommended Practice for Planning, Designing and Constructing Fixed Offshore Platforms-Working Stress Design (RP 2A-WSD).* Washington DC

Banks J. (2010). "*India rides on the wind*". Power Technology Online Magazine, Wind edition September 2010. Retrieved from: power-technology.com.

Buckingham, E. (1914). Illustration of the Use of Dimensional Equations, *On Physically Similar System*, 4(4), 345-376.

Butterfield, R., Houlsby, G.T. and Gottardi, G. (1997). Standardised sign conventions and notation for generally loaded foundations.*Geotechnique* 47(4), 1051-1054.

Byrne, B.W.(2000), *Investigation of suction caissons in dense sand.* PhD thesis, The University of Oxford.

Byrne, B.W., Houlsby, G.T. and Martin, C.M. (2002). Cyclic Loading of Shallow Foundations on Sand. *Proc. International Conference on Physical Modelling in Geotechnics (ICPMG)*, St John's, Newfoundland, Canada.

Byrne, B.W., Villalobos, F., Houlsby, G.T. and Martin, C.M. (2003). Laboratory Testing of Shallow Skirted Foundations in Sand, *Proc. BGA Int. Conf. on Foundations*, Dundee, 161.167.

Doherty J. P., Deeks A. J. (2003). Elastic response of circular footings embedded in a non-homogeneous half-space, *Géotechnique*, 53(8), 703-714.

Doherty J. P., Deeks A. J. and Houlsby, G. T. (2004). Evaluation of Foundation Stiffness Using the Scaled Boundary Finite Element Method, Computational Mechanics WCCM VI in conjunction with APCOM'04, Sept. 5-10, 2004, Beijing, China. Tsinghua University Press & Springer-Verlag.

DNV (2004). Offshore standard: Design of Offshore Wind Turbine Structures (DNV-os-j101). *Det Norske Veritas*, Hellerup, Denmark.

Gottardi, G., Houlsby, G.T. and Butterfield, R. (1999). The Plastic Response of Circular Footings on Sand under General Planar Loading, *Géotechnique* 49(4), 453-470.

Gudehus, G., and Hettler, A. (1983). Model Studies of Foundation in Granular Soil. In P. K. Banarjee, R. Butterfield (Ed.), *Development in Soil Mechanics and Foundation Engineering - 1*, 29-63.

Hettler, A. (1981). *Verschiebungen starrer und elastischer Gründungskörper in Sand bei monotoner und zyklischer Belastung*, Veröffentlichungen des Instituts für Bodenmechanik und Felsmechanik der Universität Fridericiana in Karlsruhe, Heft 90.

Houlsby, G. T., Kelly, R. B., Huxtable, J. and Byrne, B. W. (2006). Field trials of suction caissons in sand for offshore wind turbine foundations, *Géotechnique* 56(1), 3–10.

Houlsby, G.T. (1999). Model Tests on Suction Caissons in Dense Sand. Final Report on EPSRC Grant GR/L/67547, Department of Engineering Science, University of Oxford.

Houlsby, G. T. and Byrne, B.W. (2002). Suction Caisson Foundations for Offshore Wind Turbines, Journal of Wind Engineering, 26(3), 145-155.

Ibsen, L. B., Borup, M., and Hedegaard, J. (1995). *Baskarp Sand No. 15: data report 9403*. Aalborg: Aalborg Universitetscenter, Inst. for Vand, Jord og Miljøteknik, Laboratoriet for Fundering.

Huurman, M. (1996). Development of traffic induced permanent strain in concrete block pavements, *Heron* 41(1),29–52.

Ibsen, L. B. (1999). The mechanism controlling static liquefaction and cyclic strength of sand, Proc. of the International Workshop on Physics and Mechanics of Soil Liquefaction, A. A. Balkema.

Ibsen, L. B. and Bødker, L.(1994). 'Baskarp Sand No. 15', *Data Report 9301.* Geotechnical Engineering Group, Aalborg University.

Ibsen, L. B., Hanson, M., Hjort, T. and Thaarup, M. (2009). 'MC-ParameterCalibration for Baskarp Sand No. 15', DCE Technical Report No.62 .Department of Civil Engineering, Aalborg University.

Kelly, R. B., Houlsby, G. T., Byrne, B.W. (2006a). A comparison of field and laboratory tests of caisson foundations in sand and clay, *Geotechnique* 56(9), 617-626.

Kelly R.B., Houlsby G.T. and Byrne B.W. (2006b). Transient Vertical Loading of Model Suction Caissons in a Pressure Chamber, Report No. OUEL 2291/06, Department of Engineering Science, University of Oxford.

Larsen, K. A. and Ibsen, L. B.(2006). *Static experiments on bucket foundations placed in Aalborg University Sand No. 0: data report 9301.* Aalborg: Aalborg Universitetscenter, Inst. for Vand, Jord og Miljøteknik, Laboratoriet for Fundering.

Larsen, K. A. (2008). *Static Behaviour of Bucket Foundations*, PhD Thesis, Department of Civil Engineering, Aalborg University, Denmark.

Langhaar, H. L.(1951). *Dimensional Analysis and Theory of Models*, John Wiley & Sons, Inc, New York.

LeBlanc, C. (2009). *Design of Offshore Wind Turbine Support Structures: Selected Topics in the Field of Geotechnical Engineering*, PhD Thesis, Department of Civil Engineering, Aalborg University, Denmark.

LeBlanc, C., Houlsby, G. T., Byrne, B.W. (2010a). Response of stiff piles in sand to long-term cyclic lateral loading. *Geotechnique* 60(2),79–90.

LeBlanc, C., Houlsby, G. T., Byrne, B.W. (2010b). Response of stiff piles to random two-way lateral loading. *Geotechnique* 60(9),715–721.

Musial, W., Butterfield, S., Ram, B. (2006). "*Energy from Offshore Wind*",Pubblication No. NREL/CP-500-39450 NREL National Renewable Energy Laboratory.

NREL National Renewable Energy Laboratory (2010). "*Large-Scale Offshore Wind Power in United States*" (Pubblication No. NREL/TP-500-40745).

Peralta, K. P. (2010). *Investigations on the Behaviour of Large Diameter Piles Under Long-term Lateral Cyclic Loading in Cohesionless Soil*, PhD thesis, Faculty of Civil Engineering and Geodetic Science, Leibniz University, Hannover Germany.

Senders, M. (2008). *Suction Caisson in Sand as Tripod Foundations for Offshore Wind Turbines*. PhD Thesis, The University of Western Australia, Australia.

United States Department of Energy (2007). *Wind Power Today*. Retrieved from www.eere.energy.gov.

Villalobos F.A., Houlsby, G. T. and Byrne, B. W. (2004). Suction caisson foundations for offshore wind turbines, *Proc.* 5^{th} *Chilean Conference of Geotechnics, Santiago*.

Schmertmann, J. H. (1978). 'Guidelines for cone penetration test, performance and design', *US Federal Highway Administration, Washington DC, Report, FHWA-TS-78-209, 145*.

Seed, H.B. and Lee, K.L. (1967). Undrained strength characteristics of choesionless soil, *Jurnal of Soil Mechanics and Foundation Division*, ASCE, 93(6), 333-360.

Zhu, B., Houlsby, G. T., Byrne, B.W. (2010). Cyclic moment loading of suction caisson in sand, *Proceedings of the international symposium on Frontiers in offshore geotechnics II*, Perth Australia, November 2010.

Contents